

SCIENTIFIC DATA

CONFIDENTIAL

COPY OF SUBMISSION FOR PEER REVIEW ONLY

Tracking no: SDATA-23-00603B

Typical and extreme weather datasets for studying the resilience of buildings to climate change and heatwaves

Authors: Anaïs Machard (Scientific and Technical Center for Buildings), Agnese Salvati (ETSAB Barcelona School of Architecture, Polytechnic University of Catalonia), Mamak P. Tootkaboni (Politecnico di Torino), Abhishek Gaur (National Research Council Canada), Jiwei Zou (Centre for Zero Energy Building Studies, Department of Building, Civil and Environmental Engineering, Concordia University), Liangzhu Wang (Centre for Zero Energy Building Studies, Department of Building, Civil and Environmental Engineering, Concordia University), Fuad Baba (Centre for Zero Energy Building Studies, Department of Building, Civil and Environmental Engineering, Concordia University), Hua Ge (Centre for Zero Energy Building Studies, Department of Building, Civil and Environmental Engineering, Concordia University), Facundo Bre (Research Center for Computational Methods (CIMEC), UNL/CONICET), Emmanuel Bozonnet (Laboratory of Engineering Sciences for the Environment (LaSIE), La Rochelle University), Vincenzo Corrado (Politecnico di Torino), Xuan Luo (Lawrence Berkeley National Laboratory (LBNL)), Ronnen Levinson (Lawrence Berkeley National Laboratory (LBNL)), Sang Hoon Lee (Lawrence Berkeley National Laboratory (LBNL)), Tianzhen Hong (LBNL), Marcello Salles Olinger (Laboratory for Energy Efficiency in Buildings, Federal University of Santa Catarina), Roberto Lamberts (Federal University of Santa Catarina), Delphine Ramon (Department of Architecture, Faculty of Engineering Science, KU Leuven), Hoang Ngoc Dung Ngo (Building Physics and Sustainable Design, Department of Civil Engineering, KU Leuven), Abantika Sengupta (Building Physics and Sustainable Design, Department of Civil Engineering, KU Leuven), Hilde Breesch (Building Physics and Sustainable Design, Department of Civil Engineering, KU Leuven), Nicolas Heijmans (Belgian Building Research Institute (BBRI)), Jade Deltour (Belgian Building Research Institute (BBRI)), Xavier Kuborn (Belgian Building Research Institute (BBRI)), Sana Sayadi (University of Gävle), Bin Qian (Department of the Built Environment, Aalborg University), Chen Zhang (Department of the Built Environment, Aalborg University), Ramin Rahif (Sustainable Building Design Lab, Department UEE, Faculty of Applied Sciences, Université de Liège), Shady Attia (Liege University), Philipp Stern (Institute of Building Research & Innovation ZT GmbH), Peter Holzer (Institute of Building Research and Innovation (IBRI)), and Afshin Afshari (Fraunhofer Institute for Building Physics IBP)

Abstract:

We present unprecedented datasets of current and future projected weather files for building simulations in 15 major cities distributed across ten climate zones worldwide. The datasets include ambient air temperature, relative humidity, atmospheric pressure, direct and diffuse solar irradiance, and wind speed at hourly resolution, which are essential climate elements needed to undertake building simulations. The datasets contain typical and extreme weather years in the EnergyPlus weather file (EPW) format and multiyear projections in comma-separated value (CSV) format for three periods: historical (2001-2020), future mid-term (2041-2060), and future long-term (2081-2100). The datasets were generated from projections of one regional climate model, which were bias-corrected using multiyear observational data for each city. The methodology used makes the datasets among the first to incorporate complex changes in the future climate for the frequency, duration, and magnitude of extreme temperatures. These datasets, created within the IEA EBC Annex 80 “Resilient Cooling for Buildings”, are ready to be used for different types of building adaptation and resilience studies to climate change and heatwaves.

Datasets:

Repository Name	Dataset Title	Dataset Accession Number	URL	Reviewer Passcode
World Data Center for Climate	IEA EBC Annex 80	5275069	https://www.wdc-climate.de/ui/entry?acronym=WDTF_Annex80_build_v1.0	

1 Authors

2
3 Anaïs Machard^{1,2}, Agnese Salvati^{3,4}, Mamak P. Tootkaboni⁵, Abhishek Gaur⁶, Jiwei Zou⁷, Liangzhu
4 Wang⁷, Fuad Baba^{7,8}, Hua Ge⁷, Facundo Bre^{9,10}, Emmanuel Bozonnet², Vincenzo Corrado⁵, Xuan Luo¹¹,
5 Ronnen Levinson¹¹, Sang Hoon Lee¹¹, Tianzhen Hong¹¹, Marcello Salles Olinger¹², Rayner Maurício e
6 Silva Machado¹², Emeli Lalesca Aparecida da Guarda¹², Rodolfo Kirch Veiga¹², Roberto Lamberts¹²,
7 Afshin Afshari¹³, Delphine Ramon¹⁴, Hoang Ngoc Dung Ngo¹⁵, Abantika Sengupta¹⁵, Hilde Breesch¹⁵,
8 Nicolas Heijmans¹⁶, Jade Deltour¹⁶, Xavier Kuborn¹⁶, Sana Sayadi¹⁷, Bin Qian^{18,19}, Chen Zhang¹⁸, Ramin
9 Rahif²⁰, Shady Attia²⁰, Philipp Stern²¹, Peter Holzer²¹

- 10
- 11
- 12 1. Scientific and Technical Building Research Centre (CSTB), Energy and Environment
- 13 Department, Grenoble, France
- 14 2. Laboratory of Engineering Sciences for the Environment (LaSIE), La Rochelle University
- 15 3. Architecture, Energy & Environment (AiE), Polytechnic University of Catalonia
- 16 4. Brunel University London
- 17 5. Department of Energy, Politecnico di Torino, Italy
- 18 6. National Research Council Canada
- 19 7. Centre for Zero Energy Building Studies, Department of Building, Civil and Environmental
- 20 Engineering, Concordia University, Montreal, Canada
- 21 8. Architectural engineering department, Al-Zaytoonah University of Science and Technology,
- 22 Palestine
- 23 9. Institute of Construction and Building Materials, Technical University of Darmstadt,
- 24 Darmstadt, 64287, Germany
- 25 10. Centro de Investigación de Métodos Computacionales (CIMEC), UNL/CONICET, Santa Fe,
- 26 3000, Argentina
- 27 11. Lawrence Berkeley National Laboratory (LBNL), Berkeley, California, USA
- 28 12. Laboratory for Energy Efficiency in Buildings, Federal University of Santa Catarina,
- 29 Florianopolis, Brazil
- 30 13. Fraunhofer Institute for Building Physics IBP
- 31 14. Department of Architecture, Faculty of Engineering Science, KU Leuven, Belgium
- 32 15. Building Physics and Sustainable Design, Department of Civil Engineering, KU Leuven, Belgium
- 33 16. Belgian Building Research Institute
- 34 17. University of Gävle, 801 76 Gävle, Sweden
- 35 18. Department of the Built Environment, Aalborg University, Aalborg, Denmark
- 36 19. School of Mechanical Engineering, Southwest Jiaotong University, Chengdu, China
- 37 20. Sustainable Building Design Lab, Department UEE, Faculty of Applied Sciences, Université de
- 38 Liège, Belgium
- 39 21. Institute of Building Research and Innovation (IBR&I), Austria
- 40

41 **Typical and extreme weather datasets for studying the**
42 **resilience of buildings to climate change and heatwaves**

43 **Abstract**

44 We present unprecedented datasets of current and future projected weather files for building
45 simulations in 15 major cities distributed across 10 climate zones worldwide. The datasets
46 include ambient air temperature, relative humidity, atmospheric pressure, direct and diffuse
47 solar irradiance, and wind speed at hourly resolution, which are essential climate elements
48 needed to undertake building simulations. The datasets contain typical and extreme weather
49 years in the EnergyPlus weather file (EPW) format and multiyear projections in comma-
50 separated value (CSV) format for three periods: historical (2001-2020), future mid-term (2041-
51 2060), and future long-term (2081-2100). The datasets were generated from projections of
52 one regional climate model, which were bias-corrected using multiyear observational data for
53 each city. The methodology used makes the datasets among the first to incorporate complex
54 changes in the future climate for the frequency, duration, and magnitude of extreme
55 temperatures. These datasets, created within the IEA EBC Annex 80 “Resilient Cooling for
56 Buildings”, are ready to be used for different types of building adaptation and resilience
57 studies to climate change and heatwaves.
58

Background & Summary

Climate change is among the most significant challenges the global community faces in the 21st century, with direct consequences for the building sector. An increase in the magnitude, frequency, and intensity of natural hazards presents a threat to the structural integrity of the buildings. In contrast, changes in climate characteristics, such as rising temperatures and more frequent extreme heat events, present an unprecedented challenge to building designers to design buildings that can perform efficiently over their durations of use. The performance evaluation of renovated or new buildings should consider not only the current average and extreme climates but also expected future climates and extreme events. To achieve this aim, reliable weather files capturing present, future typical, and extreme weather conditions are necessary to carry out building and resilience strategies studies. To reduce the computational costs associated with running building simulation models over long periods of time, simulations are generally performed over subsets of long-term climate data, typically over one year, referred to as reference meteorological years. Depending on the application, either a typical meteorological year (TMY) or an extreme meteorological year (XMY) is chosen. Many researchers and building practitioners are currently using only future TMYs to assess the impact of climate change on building energy performance because future TMYs are easily accessible and usually built from simplified statistical methods to account for climate change (e.g., the morphing method from Belcher et al.¹). Although morphing offers a quick way to generate weather files, it does not account for complex future changes in climate variables, such as changes in the frequency and duration of extreme heat events. Therefore, the generation of future weather files containing extremes has been an ongoing challenge for the building community in the last decade. A few authors have started to use climate model outputs directly to prepare the building simulation weather files to assemble not only future TMYs but also future extreme weather files such as heatwave events (HWE) or extreme meteorological years (XMYs). For example, Nik² prepared typical and extreme weather files for Stockholm and Geneva. The typical and extreme years were selected solely based on the temperature parameter. These weather files were prepared from raw regional climate model (RCM) data from four different climate models without bias correction. Machard et al.³ prepared typical TMY and future HWE for France using data from four RCM and the Representative Concentration Pathway (RCP) 8.5 at 12.5-km spatial resolution. In Machard⁴, bias-adjustment of the RCM projections was added to the method. The typical years were assembled following ISO EN 15927-4⁵, giving equivalent weight to temperature, humidity, and solar irradiance and secondary weight to wind speed. The heatwaves were selected following the French national heatwave definition, based on daily daytime and nighttime temperatures above specific thresholds validated for France using a CORDEX dataset by Ouzeau⁶. Doutreloup et al.⁷ and Ramon et al.^{8,9} used a convection-permitting climate model at 2.8km resolution driven by the EC-Earth RCM and coupled with the land-surface scheme TERRA_URB. Based on the bias-adjusted data^{9,10}, they prepared TMYs for different locations in Belgium for an RCP 8.5 climate change scenario. They also prepared XMYs, selecting extreme months based on two parameters: temperature and solar irradiance. Gaur et al.^{11,12} used the Canadian RCM bias-corrected climate projections to prepare TMYs, typical and extreme moisture reference years, typical downscaled years, and extreme warm and extreme cold years for over 500 locations. Recently, Bass et al.¹³ published future TMYs for 18 cities in the United States based on six climate models and different socioeconomic scenarios, Shared Socioeconomic Pathways (SSP) 5 and RCP 8.5. The TMYs were assembled using data from six climate models to reduce individual model bias.

107 **Study scope**

108 Future weather files based on bias-corrected RCM predictions are not easily available to the
109 building scientific community; therefore, a large-scale international collaborative effort was
110 made to curate and produce extreme weather data covering major global cities subject to
111 extreme heat hazards by adopting a standardized procedure. This study prepares building
112 simulation weather files ready to be used by building researchers and practitioners to carry
113 out building energy simulations that are novel in the following respects:

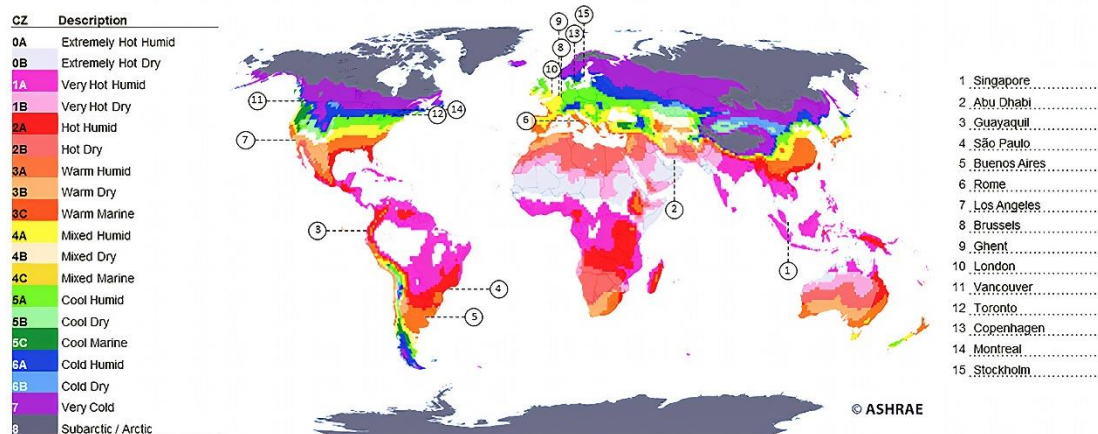
- 114
- 115 a) they have been prepared to employ a consistent methodology over 15 cities distributed
- 116 across the globe in different continents and climate types for 10 climate zones worldwide, as
- 117 defined by the American Society of Heating, Refrigerating and Air-Conditioning Engineers
- 118 (ASHRAE) 169-2013¹⁴ (Figure 1);
- 119 b) the future weather files are prepared directly from regional climate model simulation
- 120 results and hence are able to account for complex future changes such as heatwaves in the
- 121 climate variables projected for each city;
- 122 c) the use of a multivariate bias-correction method is employed to correct the bias associated
- 123 with the regional climate model simulations;
- 124 d) the reference typical years and extreme heatwave event files are provided for building
- 125 energy and overheating applications; and
- 126 e) bias-corrected multi-year projections are also made available for additional research and
- 127 other applications.

128

129 These datasets were developed for “Annex 80: Resilient Cooling of Buildings”, a research
130 project of the International Energy Agency (IEA) - Energy in Buildings and Communities
131 Programme (EBC)¹⁵, to evaluate the resilience of different passive and active cooling
132 strategies.

133

134 They are used within the framework defined in Attia et al.¹⁶ and applied in Rahif et al.¹⁷. These
135 weather files are shared to conduct climate change adaptation studies such as overheating
136 risk assessments or a rise in demand for air conditioning under future typical and extreme
137 weather conditions. The multi-year dataset is provided in comma-separated values (CSV)
138 format so that it can easily be used for adaptation studies in other fields of investigation.



139
140 *Figure 1 – 15 locations selected and ASHRAE 169-2013 climate classification¹⁴*

141 **Selected cities**

142 The weather datasets have been generated for 15 cities representative of the ten climate
143 zones of ASHRAE classification¹⁴. Cities were selected to include at least one city per zone in
144 climate zones 0 to 6 because climate change is expected to markedly increase cooling demand
145 in these zones¹⁸. Preference was given to cities with high populations and high population

146 growth. Most are in Europe, North America, and Asia due to the limitations of gathering
 147 observational data for other locations. However, these are also the continents where the most
 148 heatwave events have been recorded in the last decade¹⁹. The cities of interest and population
 149 data are presented in Table 1.
 150
 151

Table 1 - Cities analyzed and population data²⁰

ASHRAE Climate Zone (CZ)	City	Population 2022 (M)	Change % (since 2021)	Country	Continent
0A	Singapore	6.0	0.80%	Singapore	Asia
0B	Abu Dhabi	1.5	1.86%	UAE	Asia
	Guayaquil	3.1	1.62%	Ecuador	South America
2A	Sao Paulo	22.4	0.86%	Brazil	South America
3A	Buenos Aires	15.4	0.74%	Argentina	South America
3A	Rome	4.3	0.47%	Italy	Europe
3B	Los Angeles	4.0	0.05%	USA	North America
4A	Brussels	2.1	0.67%	Belgium	Europe
4A	Ghent	0.3	0.48%	Belgium	Europe
4A	London	9.5	1.22%	UK	Europe
4C	Vancouver	2.6	0.97%	Canada	North America
5A	Toronto	6.3	0.93%	Canada	North America
5A	Copenhagen	1.4	0.85%	Denmark	Europe
	Montreal	4.3	0.68%	Canada	North America
	Stockholm	1.7	1.36%	Sweden	Europe

152 Methods

153 The flow chart in Figure 2 illustrates the steps adopted to generate the weather files. In step
 154 1, raw climate data were extracted for the different weather variables that dominantly affect
 155 the thermal performance of buildings for historical and two future periods (20 years for each
 156 period). In step 2, these raw climate data were bias-corrected using observations of the
 157 different weather variables for the specific locations. In step 3, the weather files were
 158 assembled from the multiyear bias-adjusted datasets to generate (a) TMYs based on the EN
 159 ISO 15927-4 standard⁵ and (b) heatwave years (HWYs), based on the method to detect the
 160 heatwaves on a CORDEX dataset proposed by Ouzeau et al⁶, already tested for building
 161 performance simulations in²¹. Our methods are detailed in the following sections.

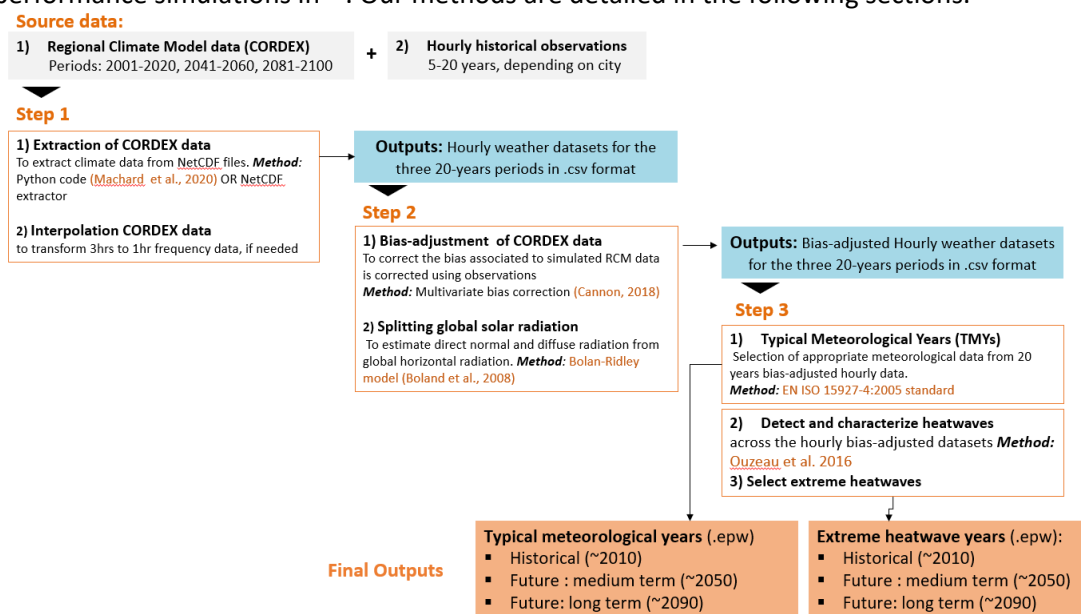


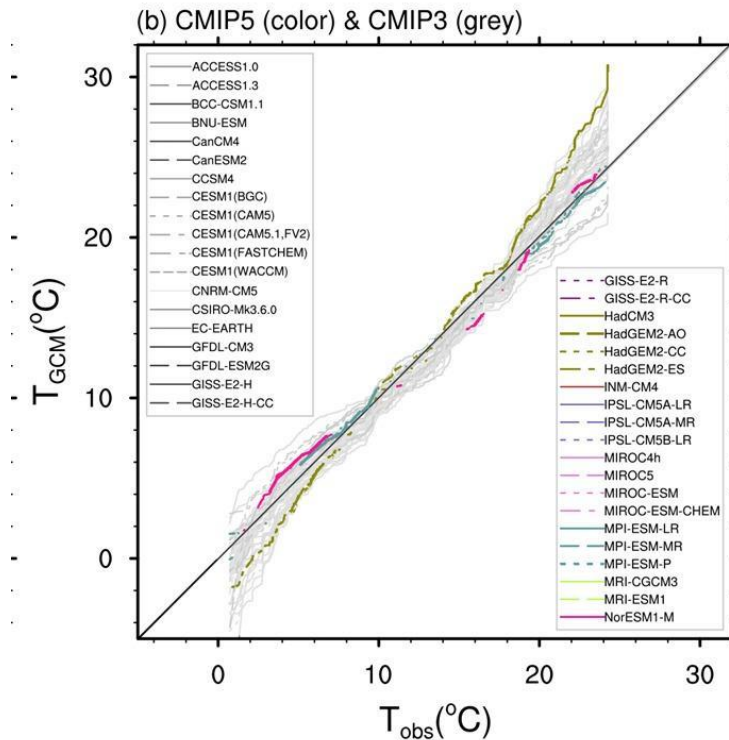
Figure 2 – Methodology used for the weather datasets generation

162
163

164 ***Boundary conditions***

165 The historical and future projected climate simulations needed to prepare the weather files
166 were taken from the Coordinated Regional Downscaling Experiment (CORDEX)^{22,23} results
167 contributed by the scientific community towards the Coupled Model Intercomparison Project
168 5th Phase (CMIP5²⁴). The CORDEX climate datasets for CMIP6²⁵ were not available at the time
169 our datasets were being prepared, so they were not considered. The future projections made
170 under the Representative Concentration Pathway (RCP) 8.5 were considered²⁶. RCP 8.5 is the
171 highest baseline scenario in which emissions rise throughout the twenty-first century. In this
172 scenario, the emissions and concentrations of greenhouse gases rise significantly over time,
173 causing a radiative forcing of 8.5 W/m² by the end of the century²⁷. This scenario is the most
174 conservative greenhouse gas emission scenario of the Coupled Model Intercomparison Project
175 5th Phase (CMIP5) which is also in line with the current emission trajectories of greenhouse
176 gases around the globe²⁸ and therefore RCP 8.5 was chosen to evaluate the worst case possible
177 in a resilience and adaptation context.

178
179 To select an appropriate climate simulation from the CORDEX database, i.e., containing data
180 for many different General Circulation Model (GCM) and Regional Climate Model (RCM)
181 combinations, we referred to the findings of McSweeney et al.²⁹. These authors analyzed all
182 GCMs participating in the CORDEX database, and three reliable GCMs with low, medium, and
183 high global equilibrium climate sensitivity (ECS) were identified as NCC-NORESM (Norwegian
184 Earth System Model, developed by the Norwegian Climate Center), MPI-ESM-LR (Max Planck
185 Institute Earth System Model for the High-Resolution Model), and HadGEM-ES (Hadley Centre
186 Global Environment Model with an Earth-System configuration), respectively. These three
187 GCMs have also been used to conduct coordinated downscaling experiments in CORDEX CORE
188 simulations³⁰. In addition to this, we conducted a review of available CORDEX simulations at
189 the needed temporal frequency (sub-daily) across different CORDEX domains encompassing
190 the different cities we are analyzing. The dry-bulb temperature projections of these three
191 climate models were compared with reference to the evaluation of the climate models report
192 (contribution of Working Group I to the IPCC AR5). Finally, the MPI-ESM-LR (GCM) and REMO
193 (RCM) combination was selected for this work as it was associated with medium global ECS,
194 was found to be the closest to the median temperature of all climate model projections (Figure
195 3) and contained simulations in the required temporal frequency (at least 3-hourly or more
196 frequent) for all domains. This selected simulation is henceforth referred to as “MPI-REMO”.
197



198
199
200
201

Figure 3 – Selection of the climate model to generate future weather datasets – Position of the temperature projection from HadGEM2-ES, MPI-ESM-LR, and NorESM1-M in comparison with other model climate projections. Modified from: Flato, Gregory, et al. 'Evaluation of climate models.' Climate change 2013³¹

202 **Downscaled climate simulations**

203 The selected GCM, MPI-ESM-LR³², is dynamically downscaled by means of an RCM, REMO^{33,34}.
204 REMO is a three-dimensional atmosphere model developed at the Max Planck Institute for
205 Meteorology in Hamburg, Germany, and currently maintained at the Climate Service Center
206 Germany (GERICS) in Hamburg. The model is based on the Europa Model, the former NWP
207 model of the German Weather Service. The prognostic variables in REMO are horizontal wind
208 components, surface pressure, air temperature, specific humidity, cloud liquid water, and ice.
209 The physical packages originate from the global circulation model ECHAM4³⁵, although many
210 updates have been introduced³⁶⁻⁴³.

211
212
213
214
215

The MPI-REMO simulations, summarized in Table 2, were of 12.5 km spatial resolution for the European domain and 25 km resolution for other domains.

Table 2 – Climate projections (model, scenario, spatial, and time frequency) used for each location.

Continent	Domain	Driving model	Downscaling method	Socio-economic scenario	Time frequency
Africa	AFR-22	MPI-ESM-LR	REMO 2015	RCP 8.5	3 HOURS
Asia	SEA-22				3 HOURS
Europe	EU-11				1 HOUR
South America	SAM-22				3 HOURS
North America	NAM-22				3 HOURS

216
217
218
219
220
221

RCM files were stored for each weather variable and for one year on the entire domain grid (a domain usually corresponds to an entire continent or parts of a continent) in NETCDF4 format. A Python code provided with this dataset was used to download the different NETCDF4 files, extract the nearest point to each city coordinates, and assemble the different weather variables and years in a single dataset. For each city, the weather variables downloaded are

222 described in Table 3. They include dry-bulb temperature, specific or relative humidity,
 223 atmospheric pressure, surface downwelling shortwave irradiance, wind speed, and cloud
 224 cover (only for Europe). Additional variables, such as rainfall, wind direction, or longwave
 225 irradiance, are also important, but they were not available for all the cities; therefore, they
 226 were not used. Data were downloaded for the three time periods referenced in Table 4.

227 *Table 3 – Weather variables downloaded from the CORDEX platform.*

EUR 11 Domain	AFR 22, NAM 22, SAM 22, and SEA 22 Domains
tas (near-surface air temperature)	tas (near-surface air temperature)
hurs (near-surface relative humidity)*	n/a
	huss (near-surface specific humidity)*
ps (surface air pressure)	ps (surface air pressure)
rsds (surface downwelling shortwave irradiance)	rsds (surface downwelling shortwave irradiance)
clt (total cloud fraction)	n/a
sfcWind (near-surface wind speed)	sfcWind (near-surface wind speed)
clt (cloud cover)	

229 *hurs is required in weather files for building performance simulations but was available only for the EU and SAM
 230 domains. For the other domains, the huss and tas variables are used to recalculate the hurs.

231 *Table 4 - 20-year periods downloaded for each variable from the CORDEX platform.*

Period Name	Years
Historical – 2010s	2001 - 2020
Mid-term future – 2050s	2041 - 2060
Long-term future – 2090s	2081 - 2100

233 ***Bias correction of climate model simulations***

234 Climate model simulations are known to have bias associated with them because of the coarse
 235 spatial resolution at which the global or regional climate simulations are conducted⁴⁴. The
 236 biases in the climate simulations, if left uncorrected, have been known to lead to incorrect
 237 descriptions of climate-driven hazards, such as floods⁴⁵ and wildfires⁴⁶. Many bias-correction
 238 methods have been discussed in literature⁴⁴. The complexity of the methods can range from
 239 methods correcting simply the mean bias⁴⁷ to methods able to perform univariate and
 240 multivariate distribution-based corrections⁴⁸. The multivariate bias-correction methods have
 241 been found most efficient in correcting bias in the marginal distribution of the climate
 242 variables, as well as the inter-relationships between the variables, and have been
 243 recommended for accurately describing hazards dependent on multiple climate variables⁴⁸.
 244 Therefore, the bias correction of raw climate variables was performed using quantile delta
 245 mapping (QDM)⁴⁹ and Multivariate Bias Correction with N-dimensional probability density
 246 function transform (MBCn)⁴⁸ methods. The QDM is a univariate bias-correction method that
 247 preserves climate model projected future changes in the quantiles of climate variables while
 248 at the same time correcting systematic biases in the quantiles. Climate model data are de-
 249 trended and then mapped onto the observations using quantile mapping. After that, future
 250 projected bias-corrected datasets are obtained by multiplying/adding to them the climate
 251 model projected future relative/additive changes in quantiles. The MBCn method extends the
 252 application of the QDM method in a multivariate context. First, individual climate variables are
 253 corrected following the QDM method. Thereafter, the dependence structure of climate
 254 variables is corrected using an iterative reshuffling process where, in each iteration, climate
 255 data are rotated by multiplying them with random orthogonal matrices, QDM is corrected and
 256 then re-correlated using inverse random matrices.

257
 258 While all climate variables were bias corrected using the MBCn method, the QDM method was
 259 used to correct global solar irradiance because our analysis shows that the reshuffling of
 260 marginally corrected global solar irradiance values, as performed in the MBCn method, breaks

261 the diurnal structure of global solar irradiance. This can subsequently lead to unrealistic values
 262 for not only global solar irradiance but also direct and diffused solar irradiance components
 263 derived from it. The calibration of MBCn/QDM methods and subsequent prediction of bias-
 264 corrected values were performed individually for each month of the year to preserve month-
 265 to-month variability in bias-corrected climate data. The methods assume that the bias is the
 266 same in the future as in the present. All years with observational data available in different
 267 cities were considered for the calibration of bias-correction methods. The length of the
 268 observational period and the variables available for each city are reported in Table 5. The
 269 observational datasets included hourly values of air temperature (tas), relative humidity
 270 (hurs), global horizontal irradiation (rsds), wind speed (sfcWind), atmospheric pressure (ps),
 271 and cloud cover (clt). Just for Sao Paulo, for which hourly values could not be found for all
 272 weather variables, the hourly values of global horizontal irradiation and wind speed were
 273 derived from daily values. Hourly values for irradiation were calculated using the Zhang-Huang
 274 solar model ⁵⁰. The regression coefficients in the model were calibrated based on the daily
 275 values using a least-squares approximation. Hourly values for wind speed were obtained by
 276 adjusting the monthly cumulative frequency distributions of historical RCM data to the
 277 observational data. Hence, each day of the RCM had its wind speed hourly values multiplied
 278 by a factor to match the cumulative frequency of the observational data daily mean values.
 279 For Abu Dhabi, data on atmospheric pressure could not be found; a static standard
 280 atmospheric pressure was used since the city is located at sea level. Note that observations of
 281 solar radiation were not available for Singapore, so its solar irradiance was not bias-corrected
 282 when the datasets were prepared.

283

284 The coordinates given in Table 5 correspond to the location of the weather station where the
 285 observations were used for bias correction for each city. The chosen weather stations are
 286 located outside of the cities, usually at airport sites; therefore, the observations and the
 287 resulting bias-corrected datasets do not account for urban heat island effects (UHI). We
 288 decided not to include urban effects in these datasets for various reasons. First, urban
 289 observations are not available for some of the cities analyzed. Secondly, the UHI is not
 290 homogeneous across a city, varying significantly depending on the different local climate zones
 291 (LCZ). Therefore, it would be necessary to create more than one urban weather file for each
 292 city, namely one for each LCZ. Furthermore, it would not be correct to use current urban
 293 observations as a reference for future UHI intensities because building density, vegetation,
 294 materials, and anthropogenic heat generation in future cities will probably change, leading to
 295 a change in UHI intensity. For all these reasons, even if the datasets refer to cities, they do not
 296 include urban effects, like most of the currently available weather datasets for building
 297 performance simulations. They can be modeled and added to the datasets in post-processing
 298 by using tools and methodologies that are discussed and referenced in the “Usage notes”
 299 section.

300

301

Table 5 - Observational data used in the bias-correction step for each city.

CZ	City	Latitude (°)	Longitude (°)	Observational data Period	Data used for bias correction					
					tas	hurs	rsds	sfcWind	ps	clt
0A	Singapore	1.37	103.98	1996-2015	x	x		x		x
0B	Abu Dhabi	24.42	54.61	2008-2012	x	x	x	x		x
		-2.15	-79.92	07-2016 – 08-2020	x	x	x	x		
2A	Sao Paulo	-23.63	-46.65	1986 - 2005	x	x	x*	x*		x
	Buenos	-34.56	-58.42	1986-2005	x	x	x	x		x
3A	Aires									

3A	Rome	41.81	12.25	2008-2017	x	x	x	x	x	
3B	Los Angeles	33.93	-118.40	2000-2019	x	x	x	x	x	
4A	Brussels	50.80	4.36	2009 - 2018	x	x	x	x		
4A	Ghent	51.05	3.73	2009-2020	x	x	x	x		x
4A	London	51.48	-0.45	1996-2015	x	x	x	x	x	x
4C	Vancouver	49.19	-123.18	1998-2017	x	x	x	x	x	
5A	Toronto	43.67	-79.40	1998-2017	x	x	x	x	x	
5A	Copenhagen	55.88	12.41	2001-2019	x	x	x	x	x	
	Montreal	45.63	-73.55	1998-2017	x	x	x	x	x	
	Stockholm	59.9	18.03	1986-2005	x	x	x	x	x	x

x* = hourly values estimated from daily values.

302 **Calculating direct and diffuse solar irradiance**

303 The Boland–Ridley model⁵¹ was used to calculate the direct and diffuse components of global
304 solar irradiance. This method is a robust and straightforward predictor model that requires
305 few inputs. The Italian National organization for standardization (UNI) has adopted this
306 reliable method to split the global solar irradiance for creating national climatic data (UNI
307 10349-1:2016)⁵². The model was also validated in a later study⁵³. The Boland–Ridley model
308 uses a logistic function (sigmoid function) for the diffuse fraction of global solar irradiance on
309 a horizontal surface based on the sky clearness index, which is the ratio of the terrestrial global
310 horizontal solar irradiance to the extraterrestrial horizontal solar irradiance. The
311 extraterrestrial horizontal solar irradiance is calculated from the solar elevation and the extra-
312 atmospheric solar irradiance received on a theoretical surface orthogonal to the sun’s rays and
313 at the Earth’s mean distance from the sun (depending on the Earth’s orbital angle). This
314 fraction includes both the horizontal direct and diffuse solar irradiance components of
315 horizontal solar irradiance. This model is used for the generation of direct-normal solar
316 irradiance⁵⁴, which is required for building energy simulation. It is computed as the ratio of the
317 direct horizontal solar irradiance to the cosine of the solar zenith angle. Calculation of direct-
318 normal solar irradiance can yield unphysical results when the direct-horizontal solar irradiance
319 and the cosine of the solar zenith angle are both small because the sun is low. In this case, a
320 threshold is introduced by applying a physical model⁵⁵ that considers the Rayleigh optical
321 depth (in the function of the air mass) and the Linke Turbidity (TL)⁵⁶, which accounts for
322 scattering and absorption by both atmospheric aerosols and atmospheric gases.

323 **Creating typical years from multiyear hourly datasets**

324 The TMYs were created using the international standard EN ISO 15927-4 – Hygrothermal
325 performance of buildings, Calculation and presentation of climatic data, Part 4: Hourly data
326 for assessing the annual energy use for heating and cooling method⁵. The procedure is
327 applicable for assessing the climate change impact on the long-term mean energy loads of
328 buildings. However, this method based on average values is not suitable for studying extreme
329 meteorological events. TMYs are constructed from 12 representative months (typical months)
330 from multiyear records. Two sets of parameters are considered for selecting the typical
331 months: primary parameters, including dry-bulb air temperature, global solar irradiance, and
332 relative humidity (or air absolute humidity, water vapor pressure, or dew point temperature),
333 and secondary parameters, including wind speed. For each primary climatic parameter, p , the
334 daily means, \bar{p} , are calculated from all multi-year records of hourly values of p (at least ten
335 years). After sorting the \bar{p} values for a specific month, m , of all the years in increasing order,
336 the cumulative distribution function is calculated for each parameter and i^{th} day as:

$$\Phi(p, m, i) = \frac{K(i)}{N + 1} \quad (1)$$

337 where $K(i)$ is the rank order of the i^{th} day and N is the number of days for a month overall
 338 multi-year records. Afterward, the cumulative function is calculated for each year of the multi-
 339 year records for a specific month, m , and specific year, y , according to equation 2:

$$F(p, y, m, i) = \frac{J(i)}{n + 1} \quad (2)$$

340
 341 where $J(i)$ is the rank order of the i^{th} day and n is the number of days for the specific month
 342 and year. Subsequently, the Finkelstein–Schafer statistic (F_s)⁵⁷ is calculated for all the primary
 343 climatic parameters for each calendar month and year of multi-year records. F_s is a goodness-
 344 to-fit statistic that proved more potent than conventional alternatives and is calculated as:
 345

$$F_s(p, y, m) = \sum_{i=1}^n |F(p, y, m, i) - \Phi(p, m, i)| \quad (3)$$

346 For each calendar month and each year, F_s values are calculated and ranked in increasing
 347 order. By calculating the total ranking (the sum of the primary parameter's ranks) for each
 348 year, three months with the lowest total ranking are selected for each calendar month. The
 349 month with the lowest deviation in wind speed (secondary parameter) is selected as the
 350 typical month to be included in the typical year. This method was applied to the 20-year bias-
 351 corrected RCM data to generate one TMY for each period. The TMYs were then converted to
 352 EnergyPlus weather files (.EPW) for use in building energy simulations. The EnergyPlus
 353 auxiliary program "weather converter" tool⁵⁸ was used for this purpose.

354 **Selecting extreme heatwaves from multi-year datasets**

355 The method proposed by Ouzeau et al.⁶ was used to select heatwaves from the 20-year
 356 periods based on high quantiles of daily temperature distributions. The method was validated
 357 for France by comparing heatwave detection on an EURO-CORDEX regional multi-model
 358 ensemble with the French SAFRAN thermal indicator, historically used by French authorities
 359 for cold spell detection. The adopted method has the advantage of applying to different cities
 360 worldwide since it is based on relative thresholds and not absolute thresholds. It detects
 361 heatwaves based on three temperature thresholds calculated from the historical multiyear
 362 period: The 99.5 threshold (99.5 percentile) is used to detect a temperature peak and a
 363 potential heatwave. The 97.5 threshold (97.5 percentile) is used to calculate the heatwave
 364 duration (days during which the temperature is above the threshold) and severity (degree-
 365 days above the threshold). If the temperature goes under this threshold for more than three
 366 consecutive days, the heatwave stops. The 95 threshold (95 percentile) is used to end the
 367 heatwave drastically if the temperature drops below this threshold. The chosen method was
 368 recently demonstrated to be the most effective in detecting and characterizing heat waves for
 369 building resilience analysis⁵⁹. The current work builds on the methodology initiated by
 370 Machard et al.³ to assemble future weather files, including heatwave for building energy and
 371 thermal performance simulations from CORDEX climate data. In the proposed approach, each
 372 heatwave is characterized by three criteria: intensity (maximum daily mean temperature °C
 373 reached during the heatwave), duration (in days), and severity (aggregated temperature
 374 above the 97.5 threshold in °C.day). Applying this method, many heatwaves were found during
 375 each multiyear period in each city. Since the purpose of the datasets is to carry out building
 376 performance resilience assessments, the three most extreme heatwaves were selected,
 377 according to these three criteria: the most intense, the most severe, and the longest
 378 heatwaves.

379 Data Records

380 The entire datasets (Table 6) produced for this work are organized into three categories:

- 381 ○ Multiyear (MY)
- 382 ○ Typical meteorological year (TMY)
- 383 ○ Heatwave year (HWY)

384 The datasets are available at the link: [https://www.wdc-](https://www.wdc-climate.de/ui/entry?acronym=WDTF_Annex80_build_v1.0)
 385 [climate.de/ui/entry?acronym=WDTF Annex80 build v1.0](https://www.wdc-climate.de/ui/entry?acronym=WDTF_Annex80_build_v1.0)⁶⁰

386
 387 The first category of files is MY datasets in CSV format. There are three MY files for each city,
 388 containing the hourly values of the bias-corrected RCM variables for each 20-year reference
 389 period. The variables included in the CSV files are air temperature (tas), near-surface relative
 390 humidity (hurs), near-surface specific humidity (huss), surface atmospheric pressure (ps),
 391 surface downwelling shortwave irradiance (rsds), and wind speed (sfcWind). Some cities have
 392 fewer variables due to missing observational data to perform the bias-correction. Cloud cover
 393 (clt) is available for London and Stockholm. The MY file name format is:
 394 "climatezone_city_MY_referenceperiod.csv". For instance: "0B_Abu Dhabi_MY_2081-2100".
 395 The MY files were used to create both TMYs and HWYs.

396 There are three TMYs per city, representing the typical meteorological conditions
 397 corresponding to historical (2001-2020), mid-term future (2041-2060), and long-term future
 398 (2081-2100) periods. The TMYs are provided in the EnergyPlus weather file (EPW) format. The
 399 EPW file details hourly dry bulb air temperature (°C), dew point temperature (°C), relative
 400 humidity (%), atmospheric pressure (Pa), global horizontal solar irradiance (Wh/m²), direct
 401 normal irradiance (Wh/m²), diffuse horizontal irradiance (Wh/m²), wind speed (m/s), and wind
 402 direction (°). For the cities of London and Stockholm, the total sky cover (tenths) is also
 403 provided. In TMYs, values for wind direction were extracted from the historical time series of
 404 METEONORM⁶¹ for each city because wind direction is needed to perform building energy
 405 simulations but is not available for all CORDEX domains. The EPW files were generated using
 406 the EnergyPlus weather converter, auxiliary software of EnergyPlus⁵⁸.

407 The file name of each TMY has the following format:
 408 "climatezone_city_TMY_referenceperiod.epw". For instance, the file
 409 "4A_London_TMY_2041-2060" is the TMY for the city of London, located in the ASHRAE
 410 climate zone 4A, for the mid-term future period (2041- 2060).

411 Finally, the HWYs are also provided in EPW format. Each city can have a maximum of nine HWY
 412 files, corresponding to the years with the most intense, most severe, and longest heatwaves
 413 found in the three reference periods. As the most intense and/or the longest heatwaves are
 414 also the most severe in many cases, the total number of HWY files is generally less than nine.
 415 The HWY file name format is
 416 "climatezone_city_HW_referenceperiod_heatwavetype_year.epw". For instance, the file
 417 "6A_Stockholm_HW_Historical_MostSevere_Longest_2002.epw" contains the most severe
 418 and longest heatwave occurring in the historical period, in 2002, in Stockholm (climate zone
 419 6A).

420
 421 *Table 6 - Datasets available for each city and data periods (Historical 2001 -2020, Mid-term future 2041-2060,*
 422 *Long-term Future (2081-2100).*

Category	Short description	Extension	Link
MY - Multiyear dataset	A file containing hourly values of 20-years bias-corrected climate data	csv	https://www.wdc-climate.de/ui/entry?acronym=WDTF Annex80 build v1.0 ⁶⁰

TMY - Typical Meteorological Year	Weather file to run building performance simulations representative of typical meteorological conditions over 20 years	epw
HWY – Heatwave year (year containing heatwaves)	Weather file to run building performance simulations including extreme heatwaves (i.e., most severe, longest, or most intense over 20 years)	epw

423 **Technical Validation**

424 For technical validation, the multiyear raw climate outputs, observations, and bias-adjusted
425 datasets were compared and analyzed. The mean values of ambient air temperature, relative
426 humidity, global solar irradiance, and wind speed in the typical years during the historical
427 period were compared to the mean values in the multiyear datasets, showing good agreement
428 in values. The extreme values of ambient air temperature for the heatwave years were
429 compared to the extreme of the multiyear datasets. An assessment of the future weather files
430 confirms that climate change will increase the mean temperature in all cities. Heatwave
431 frequency, intensity, and duration will also increase in all cities and more drastically in the four
432 hottest cities (Singapore, Abu Dhabi, Guayaquil, and Sao Paulo) analyzed.

433 ***Comparison of raw-output and bias-corrected data***

434 The validation of the bias-correction step was performed by comparing bias-corrected climate
435 estimates with observations over a validation time-period that varies from city to city
436 depending on the time period of observations available to them. The validation time period is
437 considered the period overlapping between observational and historical time-periods. This
438 allowed us to make use of the entire length of observational data available in different cities
439 for performing validation of bias-correction methods. The validation results show that the
440 QDM/MBCn methods were able to reduce the bias associated with RCM simulations
441 effectively. This can be seen from the results presented in Table 7, in which mean climate
442 statistics from observations, raw RCM, and bias-corrected (bc) RCM are presented for the
443 validation time period. The results show that the projected temperature, solar irradiance,
444 wind speed, and relative humidity from raw RCMs have noticeable bias, which is reduced by
445 the application of the bias-correction step. For instance, RCM over-predicts the mean
446 temperature in Singapore by 0.5°C, which is effectively eliminated after the bias correction.
447 Table 8 presents the standard deviation of observations (OBS), RCM-raw, and RCM-bs for
448 these four climate variables, which also shows the bias reduction between OBS and bias-
449 corrected RCM data. Not only is the bias correction effective in correcting bias in average
450 climate characteristics over the cities, but it also reduces bias across the whole distribution of
451 climate variables. This is evident from Figure 4, in which probability density functions (PDFs)
452 of temperature, wind speed, and relative humidity from observations (grey), raw RCM (blue),
453 and bias-corrected RCM (red) datasets are presented for Singapore, London, and Toronto.
454 PDFs of raw RCM are effectively adjusted by the bias-correction procedure to mimic the PDFs
455 of observations. This is true not only for temperature but also for relatively more complex
456 variables such as wind speed, highlighting the effectiveness of the bias-correction step in
457 simulating realistic estimates of a range of climate variables considered in this study.

458
459
460
461
462

Table 7 - Mean temperature, solar irradiance, wind speed, and relative humidity in the cities over the validation time period.

CZ	City	Temperature (°C)			Solar irradiance (W/m ²)			Wind speed (m/s)			Relative humidity (%)		
		OBS	RCM (raw)	RCM (bc)	OBS	RCM (raw)	RCM (bc)	OBS	RCM (raw)	RCM (bc)	OBS	RCM (raw)	RCM (bc)
0A	Singapore	27.8	28.1	27.7	-	-	-	1.9	4.7	2.0	83.8	74.1	83.3
0B	Abu Dhabi	27.6	29.0	27.6	237.9	246.7	238.1	3.2	4.0	3.2	60.0	55.5	60.2
1A	Guayaquil	27.0	27.1	27.0	263.1	218.4	266.9	1.7	1.9	1.8	74.6	77.4	74.3
2A	Sao Paulo	19.3	9.0	19.3	188.6	265.8	188.6	6.1	2.0	6.1	80.6	44.7	80.6
3A	Buenos Aires	18.0	19.1	17.7	191.4	197.5	190.0	4.5	4.5	4.4	72.1	66.9	72.3
3A	Rome	16.3	16.5	16.3	187.8	163.9	188.0	3.6	2.7	3.6	72.5	70.0	72.4
3B	Los Angeles	16.7	20.7	16.7	215.1	223.3	214.7	1.7	2.4	1.7	72.3	57.5	72.4
4A	Brussels	10.8	11.1	10.8	127.2	109.1	127.2	3.6	3.7	3.6	78.5	82.0	78.5
4A	Ghent	11.1	11.3	11.1	126.4	110.3	126.3	3.4	4.1	3.4	78.6	82.8	78.7
4A	London	11.6	11.1	11.8	118.8	106.8	117.5	4.2	2.8	4.0	75.5	79.5	75.7
4C	Vancouver	10.1	7.8	10.6	142.7	130.5	153.7	3.7	3.3	4.4	78.9	69.2	74.5
5A	Toronto	9.2	6.6	7.8	159.0	146.6	153.7	4.4	3.6	4.4	69.3	79.1	69.2
5A	Copenhagen	8.8	9.3	8.8	118.2	102.1	118.2	3.3	4.6	3.3	82.4	84.9	82.4
6A	Montreal	7.7	4.9	7.8	153.8	134.8	153.7	4.4	3.5	4.4	69.2	83.6	69.2
6A	Stockholm	6.6	6.4	6.6	116.5	92.9	116.6	3.9	3.0	3.9	79.6	86.0	79.6

463
464
465
466

Table 8 - Standard deviation of temperature, solar irradiance, wind speed, and relative humidity in the cities over the validation time period.

CZ	City	Temperature (°C)			Solar irradiance (W/m ²)			Wind speed (m/s)			Relative humidity (%)		
		OBS	RCM (raw)	RCM (bc)	OBS	RCM (raw)	RCM (bc)	OBS	RCM (raw)	RCM (bc)	OBS	RCM (raw)	RCM (bc)
0A	Singapore	2.2	1.5	2.1	-	-	-	1.6	1.9	1.6	9.9	6.9	10.0
0B	Abu Dhabi	7.9	7.7	7.9	312.4	326.9	313.2	2.2	2.1	2.2	20.4	21.4	20.5
1A	Guayaquil	3.4	3.3	3.4	380.8	312.1	382.3	1.0	0.9	1.0	12.4	14.4	12.0
2A	Sao Paulo	4.7	6.5	4.7	256.4	362.4	256.4	2.9	1.1	3.0	256.4	362.4	256.4
3A	Buenos Aires	5.6	5.1	5.7	283.5	297.3	282.5	2.4	1.9	2.4	15.2	16.3	15.4
3A	Rome	7.1	7.3	7.1	270.4	255.6	270.4	2.2	1.7	2.2	16.7	17.6	16.7
3B	Los Angeles	4.4	7.4	4.4	295.9	310.6	296.1	1.0	1.3	1.0	22.3	22.8	22.2
4A	Brussels	6.8	6.8	6.8	196.2	201.0	196.1	1.8	1.8	1.8	14.3	14.1	14.3
4A	Ghent	6.8	6.6	6.8	201.0	193.5	200.6	1.9	2.0	1.9	15.4	13.5	15.2
4A	London	6.1	6.3	6.1	193.1	195.9	191.3	2.2	1.2	2.2	15.9	14.0	15.7
4C	Vancouver	5.3	12.0	6.0	231.2	511.1	235.4	2.3	2.2	2.5	13.0	16.8	12.7
5A	Toronto	10.9	9.2	12.0	241.4	222.8	235.4	2.7	1.8	2.5	16.2	14.5	16.8
5A	Copenhagen	7.2	6.3	7.2	196.0	191.4	196.1	2.1	2.2	2.1	15.4	11.7	15.4
6A	Montreal	12.0	8.7	12.0	235.4	213.4	253.4	2.6	1.8	2.5	16.8	13.4	16.8
6A	Stockholm	7.9	7.7	7.9	184.7	178.0	184.7	1.7	1.4	1.7	14.6	11.7	14.6

467

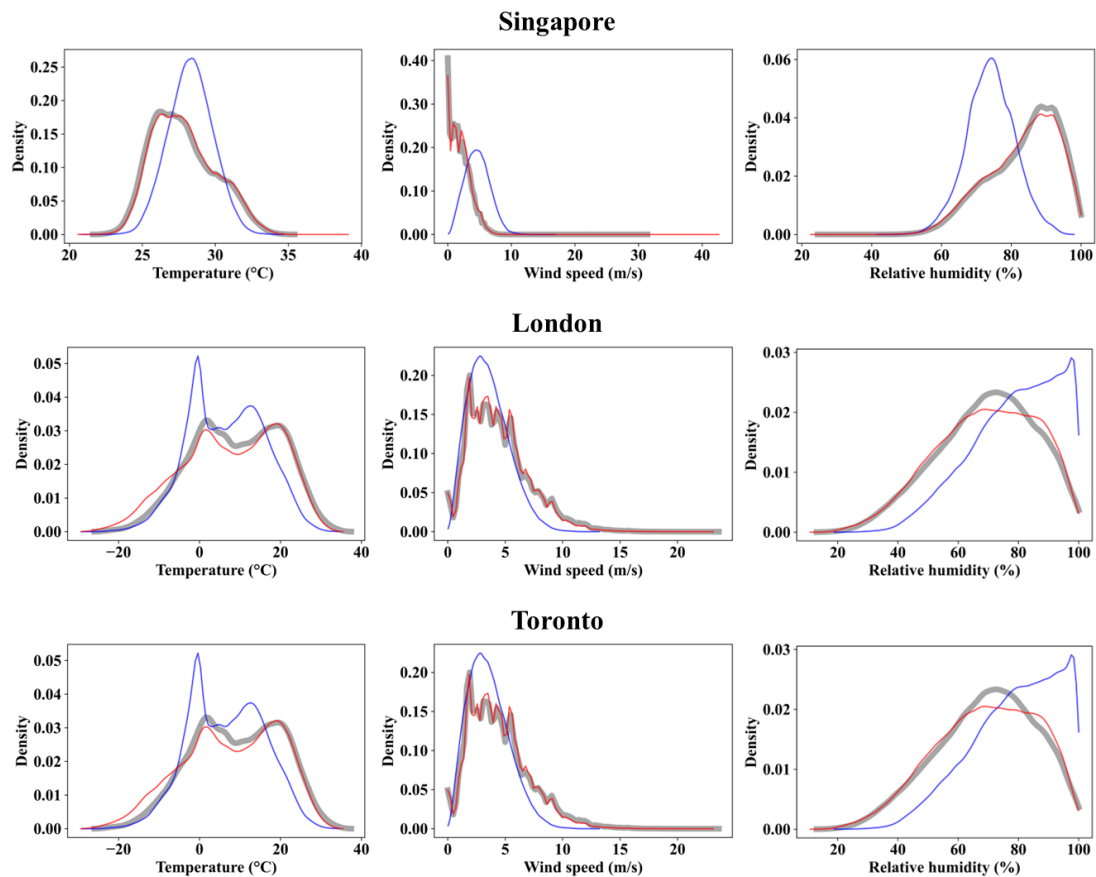


Figure 4 - Probability density functions of temperature, wind speed, and relative humidity in Singapore, London, and Toronto from observations (grey), raw RCM (blue), and bias-corrected RCM (red) datasets over the validation time period.

468
469
470
471

472 **Projected changes in weather variables over multi-year (MY)** 473 **future periods**

474 The values of mean temperature, solar irradiance, wind speed, and relative humidity over the
475 2010s, 2050s, and 2090s for all cities are presented in Table 9. In general, between the
476 historical period (the 2010s) and the two future time periods (2050s, 2090s), mean
477 temperatures are projected to increase in all cities located in different climate zones (CZs). In
478 most cities, the increase in MY by the 2050s is about 1 °C, while it will be about 2-3 °C by the
479 2090s, with the largest increase of 4.2 °C in Abu Dhabi (CZ: 0B – Extremely Hot Dry) and the
480 smallest increase of 1.6 °C in Buenos Aires (CZ: Warm Humid). Mean temperature increases
481 within the same ASHRAE climate zone are consistent: in zone ASHRAE CZ: 4A - Mixed Humid,
482 the temperature increase in Brussels, Ghent, and London are about 0.8 °C, 0.7 °C, and 0.7 °C
483 between MY-2050s and MY-2010s, and of 2.6 °C, 2.6 °C, and 2.5 °C between MY-2090s and
484 MY-2010s. Global solar irradiance is projected to decrease in the majority of the cities, with
485 the largest decrease of 12.8 W/m² by the 2090s is projected for Stockholm (CZ: Cold Humid),
486 whereas a slight increase of 0.6 W/m² is projected for Abu Dhabi (CZ 0B -: Extremely Hot Dry).
487 Such a reduction in future solar irradiance was also found in other studies^{47, 63}. According to
488 Cutforth and Judiesch⁶⁴, this can be the consequence of two factors: 1) higher attenuation of
489 solar irradiance from increased aerosol concentrations and sometimes from increasing
490 cloudiness, and 2) an increase in annual number of precipitation events. These assumptions
491 are coherent since the irradiance is not decreasing in Abu Dhabi, for which cloud cover is very
492 low. However, this trend in decreasing global solar irradiance cannot be generalized. It can be
493 due to a coarse representation of rain and cloud events at the model spatial resolution (25 or
494 50 km depending on the CORDEX domain) and to potential biases for this climate parameter

495 in the selected climate model. In terms of wind speed and relative humidity, a general change
 496 is not observed. Most cities have minimal change in wind projections in the future: The largest
 497 decrease of 0.4 m/s in wind speed is projected for Buenos Aires (CZ: Warm Humid), whereas
 498 the largest increase of 0.3 m/s in wind speed is projected for Sao Paulo (CZ: Hot Humid). Finally,
 499 the largest variability in the sign of projected future change is obtained for relative humidity.
 500 While the cities of Singapore (CZ: 0A - Extremely Hot Humid), Guayaquil (CZ: 1A - Very Hot
 501 Humid), Buenos Aires (CZ: 3A - Warm Humid), Los Angeles (CZ: 3B - Warm Dry) are projected
 502 to experience increases in relative humidity of up to 5%, the cities of Sao Paulo (CZ: 2A - Hot
 503 Humid) and Abu Dhabi (CZ: 0B - Extremely Hot Dry) are projected to experience future
 504 decreases of up to 4%. Smaller future changes in relative humidity are projected for other
 505 cities such as Montreal and Stockholm (CZ: 6A - Cold Humid) as well as Ghent, Brussels, and
 506 London (CZ: 4A - Mixed Humid and 5A – Cold Humid).

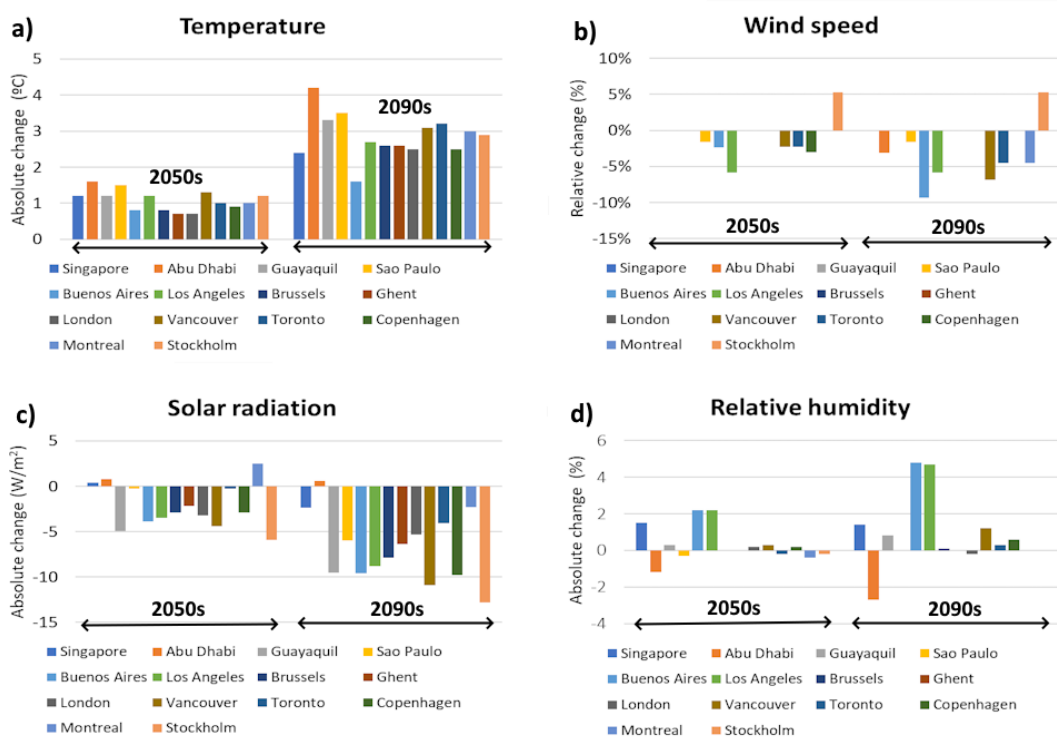
507
 508
 509
 510
 511
 512

Table 9 – 20-year mean temperatures, solar irradiance, wind speed, and relative humidity in the cities over the 2010s, 2050s, and 2090s time periods obtained from multi-year bias-corrected RCM data. Cells with future projected increases (decreases) in climate variables are highlighted in red (green). Grey color means no change. Values in brackets represent the change (absolute value for temperature, solar irradiance, and relative humidity, relative change for wind speed) between the selected term and the 2010s.

CZ	City	Temperature (°C)			Solar irradiance (W/m ²)			Wind speed (m/s)			Relative humidity (%)		
		2010s	2050s	2090s	2010s	2050s	2090s	2010s	2050s	2090s	2010s	2050s	2090s
0A	Singapore	27.9	29.1 (1.2)	30.3 (2.4)	168.6	169.0 (0.4)	166.2 (-2.4)	2.0	2.0 (0.0%)	2.0 (0.0%)	83.2	84.7 (1.5)	84.6 (1.4)
0B	Abu Dhabi	27.7	29.3 (1.6)	31.9 (4.2)	240.3	241.1 (0.8)	240.9 (0.6)	3.2	3.2 (0.0%)	3.1 (-3.1%)	60.0	58.8 (-1.2)	57.3 (-2.7)
1A	Guayaquil	26.9	28.1 (1.2)	30.2 (3.3)	263.0	258.1 (-4.9)	253.5 (-9.5)	1.7	1.7 (0.0%)	1.7 (0.0%)	74.9	75.2 (0.3)	75.7 (0.8)
2A	Sao Paulo	19.8	21.3 (1.5)	23.3 (3.5)	188.8	188.5 (-0.3)	182.8 (-6.0)	6.1	6.0 (-1.6%)	6.0 (-1.6%)	80.3	80.0 (-0.3)	80.3 (0.0)
3A	Buenos Aires	17.9	18.7 (0.8)	19.5 (1.6)	188.4	184.5 (-3.9)	178.8 (-9.6)	4.3	4.2 (-2.3%)	3.9 (-9.3%)	73.5	75.7 (2.2)	78.3 (4.8)
3A	Rome	16.1	17.1 (1.0)	19.6 (2.5)	187.7	183.7 (-4.0)	185.7 (-2.0)	3.6	3.6 (0.0%)	3.5 (-2.8%)	72.1	73.3 (1.2)	71.4 (-0.7)
3B	Los Angeles	16.7	17.9 (1.2)	19.4 (2.7)	214.7	211.2 (-3.5)	205.9 (-8.8)	1.7	1.6 (-5.9%)	1.6 (-5.9%)	72.4	74.6 (2.2)	77.1 (4.7)
4A	Brussels	10.8	11.6 (0.8)	13.4 (2.6)	126.2	123.3 (-2.9)	118.3 (-7.9)	3.6	3.6 (0.0%)	3.6 (0.0%)	78.6	78.6 (0.0)	78.7 (0.1)
4A	Ghent	11.0	11.7 (0.7)	13.6 (2.6)	108.1	105.9 (-2.2)	101.7 (-6.4)	4.2	4.2 (0.0%)	4.2 (0.0%)	83.1	83.1 (0.0)	83.1 (0.0)
4A	London	12.0	12.7 (0.7)	14.5 (2.5)	118.4	115.2 (-3.2)	113.1 (-5.3)	4.0	4.0 (0.0%)	4.0 (0.0%)	75.1	75.3 (0.2)	74.9 (-0.2)
4C	Vancouver	7.8	9.1 (1.3)	10.9 (3.1)	153.8	149.4 (-4.4)	142.9 (-10.9)	4.4	4.3 (-2.3%)	4.1 (-6.8%)	69.2	69.5 (0.3)	70.4 (1.2)
5A	Toronto	7.9	8.9 (1.0)	11.1 (3.2)	153.7	153.4 (-0.3)	149.6 (-4.1)	4.4	4.3 (-2.3%)	4.2 (-4.6%)	68.9	68.7 (-0.2)	69.2 (0.3)
5A	Copenhagen	8.8	9.7 (0.9)	11.3 (2.5)	117.8	114.9 (-2.9)	108.0 (-9.8)	3.3	3.2 (-3.0%)	3.3 (0.0%)	82.4	82.6 (0.2)	83.0 (0.6)
6A	Montreal	7.9	8.9 (1.0)	10.9 (3.0)	154.3	156.8 (2.5)	152.0 (-2.3)	4.4	4.4 (0.0%)	4.2 (-4.6%)	69.0	68.6 (-0.4)	69.0 (0.0)
6A	Stockholm	7.7	8.9 (1.2)	10.6 (2.9)	116.4	110.5 (-5.9)	103.6 (-12.8)	3.8	4.0 (5.3%)	4.0 (5.3%)	79.1	78.9 (-0.2)	79.1 (0.0)

513
 514
 515
 516
 517

The change between future 20-year periods (2050s and 2090s) compared to the present period (2010s) is presented for the mean temperature, mean solar irradiance, mean wind speed, and mean relative humidity in Figure 5.



519
520
521

Figure 5 - Changes in climatic variables from the 2010s to 2050s and 2090s: a: absolute change for temperature, b: relative change in wind speed, c: absolute change in solar radiation, d: absolute change in relative humidity

522
523

524 Table 10 highlights changes at the 99 percentiles of the multi-year distributions. A sharp
525 increase in temperatures is witnessed, especially in the four hottest cities, with changes up to
526 +5.8 °C by the end of the century (i.e., Sao Paulo). For the solar irradiance, wind speed, and
527 relative humidity, similar trends are observed for the mean values.

528
529
530
531

Table 10 - 20-year 99% temperatures, solar irradiance, wind speed, and relative humidity in the cities over the 2010s, 2050s, and 2090s time periods obtained from multi-year bias-corrected RCM data. Cells with future projected increases (decreases) in climate variables are highlighted in red (green). Grey color means no change.

CZ	City	Temperature (°C)			Solar irradiance (W/m ²)			Wind speed (m/s)			Relative humidity (%)		
		2010s	2050s	2090s	2010s	2050s	2090s	2010s	2050s	2090s	2010s	2050s	2090s
0A	Singapore	33.0	34.4 (1.4)	38.2 (5.2)	965.1	960.0 (-5.1)	949.4 (-15.7)	6.2	6.2 (0.0%)	6.0 (-3.3%)	99.4	100 (0.6)	100 (0.6)
0B	Abu Dhabi	44.3	46.4 (2.1)	49.5 (5.2)	940.3	934.9 (-5.4)	927.3 (-13.0)	9.2	9.1 (-1.1%)	9.0 (-2.2%)	95.1	94.8 (-0.3)	94.4 (-0.7)
1A	Guayaquil	34.6	35.7 (1.1)	37.8 (3.2)	1,296.5	1,281.0 (-15.5)	1,260.3 (-36.2)	4.7	4.7 (0.0%)	4.5 (-4.4%)	99.0	99.0 (0.0)	99.0 (0.0)
2A	Sao Paulo	31.0	33.6 (2.6)	36.8 (5.8)	895.6	891.4 (-4.2)	881.7 (-13.9)	13.9	14.1 (1.4%)	14.5 (4.1%)	100	100 (0.0)	97.7 (-2.3)
3A	Buenos Aires	29.5	30.0 (0.5)	30.6 (1.1)	1,011.0	1,002.8 (-8.2)	994.7 (-16.3)	11.1	10.9 (-1.8%)	10.4 (-6.7%)	100	100 (0.0)	100 (0.0)
3A	Rome	30.6	32.0 (1.4)	35.9 (5.3)	906.0	898.8 (-9.2)	892.0 (-14)	10.5	10.5 (0.0%)	10.4 (-1.0%)	100	100 (0.0)	100 (0.0)
3B	Los Angeles	28.1	29.8 (1.7)	31.0 (2.9)	956.0	946.1 (-9.9)	934.9 (-21.1)	4.2	4.2 (0.0%)	4.2 (0.0%)	100	100 (0.0)	100 (0.0)
4A	Brussels	26.4	28.0 (1.6)	29.3 (2.9)	759.0	749.7 (-9.3)	733.1 (-25.9)	8.7	9.0 (3.3%)	9.0 (3.3%)	98.9	98.8 (-0.1)	98.8 (-0.1)

4A	Ghent	26.9	28.1 (1.2)	29.5 (2.6)	779.4	771.6 (-7.8)	753.8 (-25.6)	9.6	9.8 (2.0%)	9.9 (3.0%)	100	100 (0.0)	100 (0.0)
4A	London	26.7	27.8 (1.1)	29.9 (3.2)	779.4	770.6 (-8.8)	763.6 (-15.8)	10.5	10.7 (1.9%)	10.6 (0.9%)	98.0	98.0 (0.0)	98.0 (0.0)
4C	Vancouver	28.9	30.4 (1.5)	31.7 (2.8)	882.5	872.7 (-9.8)	858.6 (-23.9)	11.8	11.6 (-1.7%)	11.5 (-2.6%)	98.3	98.1 (-0.2)	98.1 (-0.2)
5A	Toronto	29.0	30.7 (1.7)	32.9 (3.9)	882.4	879.6 (-2.8)	863.6 (-18.8)	11.9	11.7 (-1.7%)	11.6 (-2.6%)	98.1	98.2 (0.1)	98.2 (0.1)
5A	Copenhagen	24.7	25.7 (1.0)	26.4 (1.7)	779.1	770.9 (-8.2)	757.8 (-21.3)	9.2	9.2 (0.0%)	9.3 (1.1%)	100	100 (0.0)	100 (0.0)
6A	Montreal	29.0	30.0 (1.0)	31.8 (2.8)	883.6	881.0 (-2.6)	872.8 (-10.8)	11.9	11.7 (-1.7%)	11.4 (-4.4%)	97.8	97.9 (0.1)	97.3 (-0.5)
6A	Stockholm	24.2	24.9 (0.7)	25.6 (1.4)	699.0	696.3 (-2.7)	682.7 (-16.3)	8.4	8.7 (3.4%)	8.8 (4.5%)	99.0	99.0 (0.0)	98.9 (-0.1)

532 **Projected changes in weather variables of typical**
533 **meteorological years (TMY) for building performance**
534 **simulations**

535 Table 11 presents the values of mean temperatures, solar irradiance, wind speed, and relative
536 humidity in the three typical meteorological years (TMY) generated from each 20-year dataset.
537 The projected changes in climate variables in the future TMYs are generally consistent with
538 those resulting from the comparison of the 20-year datasets. This means that the TMYs are
539 indeed representative of the climate projections over an interval (i.e., 20 years) and thus
540 suitable for assessing the impact of climate change on building energy loads.

541

542 *Table 11 - Mean temperatures, solar irradiance, wind speed, and relative humidity in the three TMYs weather files*
543 *generated based on the bias-corrected 20-years datasets for each city.*

CZ	City	Temperature (°C)			Solar irradiance (W/m ²)			Wind speed (m/s)			Relative humidity (%)		
		2010s	2050s	2090s	2010s	2050s	2090s	2010s	2050s	2090s	2010s	2050s	2090s
0A	Singapore	27.9	29.1	30.3	163.7	167.5	165.6	2.1	2.0	2.0	82.7	84.8	84.8
0B	Abu Dhabi	27.9	29.4	31.7	233.9	235.5	234.7	3.2	3.2	3.1	59.7	58.4	57.7
1A	Guayaquil	27.1	28.5	30.4	255.5	243.4	232.5	1.7	1.8	1.6	73.4	71.8	75.8
2A	Sao Paulo	19.8	21.3	23.1	190.9	193.3	183.8	6.0	6.0	6.0	80.3	80.6	80.6
3A	Buenos Aires	17.8	18.9	19.5	192.8	190.1	182.9	4.3	4.1	3.9	73.5	74.9	78.5
3A	Rome	16.1	17.2	19.5	189.4	185.6	187.2	3.6	3.6	3.6	73.2	72.5	70.5
3B	Los Angeles	16.7	17.8	19.3	219.8	210.1	206.1	1.7	1.6	1.6	71.4	75.5	79.0
4A	Brussels	11.2	11.4	13.5	124.9	119.9	118.8	3.7	3.7	3.7	79.5	78.6	78.4
4A	Ghent	10.9	11.5	13.3	124.5	119.0	118.5	3.4	3.5	3.4	79.0	79.6	79.2
4A	London	12.1	12.7	14.2	116.9	114.4	110.6	4.1	4.0	4.0	75.1	75.2	76.0
4C	Vancouver	7.7	9.3	10.7	156.3	147.2	147.8	4.7	4.2	4.0	67.6	71.5	76.0
5A	Toronto	8.2	9.3	11.4	155.1	155.4	149.8	4.3	4.4	4.2	71.0	67.4	69.5
5A	Copenhagen	9.0	9.7	11.2	119.8	113.1	107.4	3.3	3.2	3.4	81.2	83.3	83.0
6A	Montreal	7.9	9.0	10.8	153.9	156.5	149.0	4.3	4.7	4.4	69.8	70.1	69.9
6A	Stockholm	7.9	8.9	10.7	119.5	111.9	108.8	3.8	3.9	4.0	79.7	79.7	78.4

544

545 The air temperature is consistently higher in the future weather files for all the cities, with a
546 higher increase in the long-term (2090s) future TMY than in the mid-term (2050s) future TMY.
547 The 2090s-TMY of Abu Dhabi (CZ: 0B Extremely Hot Dry) has the largest increase in

548 temperature of 3.8 °C whereas the TMY of Buenos Aires (CZ: 3A Warm Humid) has the smallest
549 increase of 1.7 °C for the same period. Many cities are projected to have significantly higher
550 increases in temperature in the long-term than in the mid-term (e.g., Brussels, Ghent, and
551 London). These results are in close agreement with the changes obtained from the 20-year
552 projections. As for the MYs, global solar irradiance will be reduced in the future TMYs of most
553 cities. This is also in agreement with the 20-year projections. The 2090-TMY of Guayaquil (CZ:
554 1A Very Hot Humid) has the largest decrease in solar irradiance (23.0 W/m²). The TMYs with
555 slight increases in long-term global solar irradiance are those of Singapore (CZ: 0A Extremely
556 Hot Humid) and Abu Dhabi (CZ: 0B Extremely Hot Dry). Regarding wind speed, the changes
557 between the 2010s, 2050s, and 2090s weather files are minimal. The 2090s-TMY of Vancouver
558 (CZ: 4C Mixed Marine) has the largest decrease in mean wind speeds of 0.7 m/s.
559 Finally, the future TMYs reflect a high variability in the sign of future changes in relative
560 humidity in agreement with the results of the 20-years projections. The cities of Singapore (CZ:
561 0A Extremely Hot Humid), Guayaquil (CZ: 1A Very Hot Humid), Buenos Aires (CZ: 3A Warm
562 Humid), Los Angeles (CZ: 3B Warm Dry) and Vancouver (CZ: 4C Mixed Marine) have an
563 absolute increase in relative humidity up to 8% in the 2090-TMYs while Abu Dhabi (CZ: 0B
564 Extremely Hot Dry) has a reduction of relative humidity in the 2090-TMY of 2%. The other cities
565 have relatively smaller changes in relative humidity in future TMYs. This variability can be
566 explained by two phenomena. On the one hand, there is general warming, and warmer air can
567 hold more water vapor (air can contain about 7% more moisture for every 1 °C temperature
568 increase according to the Clausius-Clapeyron equation). On the other hand, global warming
569 leads to more evaporation of water and, thus, an increase in specific humidity. Therefore, to
570 keep relative humidity the same, specific humidity must also increase by 7% per °C of warming.
571 However, the oceans are warming more slowly than the land surface, which also means that
572 not enough moisture has evaporated, and relative humidity has, therefore, been reduced.

573 ***Projected changes in heatwaves (HWY) and selected extreme***
574 ***heatwaves for building performance simulations***

575 Table 12 presents the three thresholds calculated for each city from the 20-year bias-adjusted
576 historical daily temperatures data from 2001 to 2020 for heatwave selection. The relative
577 thresholds are similar for all cities, resulting in different absolute thresholds presented in Table
578 12. Abu Dhabi is the city with the highest daily mean temperatures. The three European cities
579 in CZ 4A have equivalent thresholds. For the colder climate zones 5A and 6A, Toronto and
580 Montreal in the eastern of Canada have similar thresholds, while European cities Copenhagen
581 and Stockholm also have similar thresholds.

582
583
584

Table 12 - Thresholds used over the historical period 2010s (2001-2020) for heatwave selection and number of heatwaves found per period in each city

CZ	City	CORDEX Domain	Threshold to detect heatwaves over 2010s			Number of heatwaves detected		
			95 Threshold (°C)	97.5 Threshold (°C)	99.5 Threshold (°C)	2010s	2050s	2090s
0A	Singapore	SEA	30.4	30.9	31.7	7	58	136
0B	Abu Dhabi	SEA	37.1	38.1	39.3	5	47	61
1A	Guayaquil	AFR	29.3	29.8	30.8	8	40	207
2A	Sao Paulo	SAM	25.3	26.3	28.3	7	87	172
3A	Buenos Aires	SAM	25.3	26.4	28.0	6	19	32
3A	Rome	EUR	25.6	26.4	27.9	7	21	36
3B	Los Angeles	NAM	22.0	22.8	24.4	3	40	81
4A	London	EUR	20.6	21.9	24.3	6	16	46
4A	Brussels	EUR	20.4	22.0	24.6	9	14	36

4A	Ghent	EUR	20.2	21.8	25.0	7	20	33
4C	Vancouver	NAM	24.0	25.3	27.5	8	23	54
5A	Toronto	NAM	23.3	24.2	25.7	4	39	85
5A	Copenhagen	EUR	18.7	20.1	22.3	10	19	23
6A	Montreal	NAM	23.3	24.1	25.5	4	38	88
6A	Stockholm	EUR	18.6	19.8	21.7	9	25	27

585

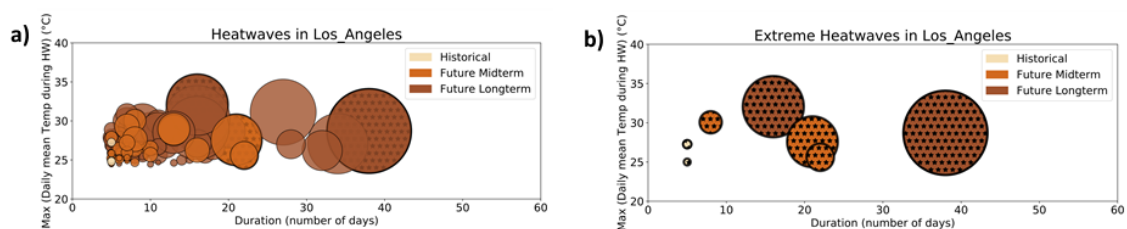
586 Table 12 also presents the evolution in the number of heatwaves found during each 20-year
587 period. While between 3 and 10 heatwaves are found during the historical period, depending
588 on the cities, a substantial increase in heatwave numbers in the future will be observed in all
589 cities. By 2050, the increase is more pronounced in cities in the four hottest climate zones,
590 followed by cities in North America and then in Europe. Still, in the twenty-year period, every
591 city displays at least one heatwave per summer on average by the mid-century. By the end of
592 the century, the three cities in hot-humid climate zones (Singapore, Guayaquil, and Sao Paulo)
593 showcase an impressive number of heatwaves, beyond a hundred, which would be equivalent
594 to an average of five heatwaves per summer. In these cities, due to the large increase in
595 temperatures, the heatwaves thresholds are exceeded many times during the same summer.
596

597 An illustration of the selection of the extreme heatwaves (the most intense, the most severe,
598 and the longest of each period) is made in Figure 6 for the city of Los Angeles. A bubble
599 represents a heatwave, which size is linked to its severity. Figure 6 a) illustrates well the
600 tremendous increase throughout the century and the diversity of heatwaves that are found as
601 well. In comparison with the historical period, during which only very short heatwaves of five
602 days are witnessed, in the mid-term future, longer heatwaves that are both less or more
603 intense than the most intense heatwave of the historical period are found. By the end of the
604 century, heatwaves are more severe and also longer. In Figure 6 b), the three most extreme
605 heatwaves, the ones that are selected for future periods, are highlighted. During the 2050s:

- 606 ○ the most intense heatwave is 8 days long with an intensity of 30.1 °C and a severity of
607 14.2 °C.d;
- 608 ○ the most severe heatwave is 21 days long with an intensity of 27.6 °C and a severity of
609 32.4 °C.d;
- 610 ○ the longest heatwave is 22 days long with an intensity of 25.6 °C and a severity of
611 17.5 °C.d;

612 During the 2100s, only two extreme heatwaves are selected:

- 613 ○ the most intense, which is also the most severe: intensity of 32.1 °C, duration of 16
614 days, and severity of 39.1 °C.d;
- 615 ○ the longest, which is 38 days long with an intensity of 28.7 °C and a severity of 53.6 °C.d
616

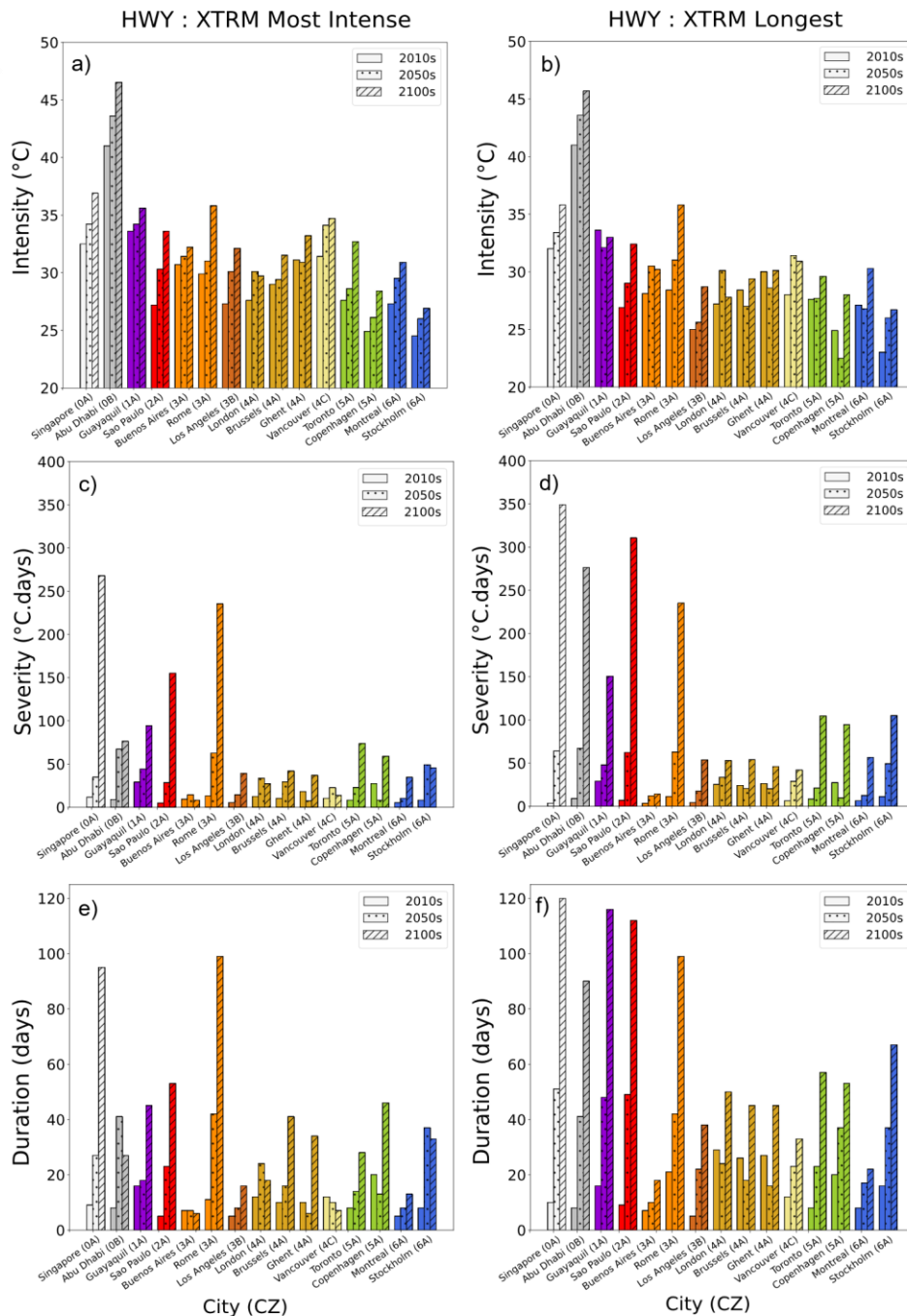


617

618

Figure 6 – Heatwaves in Los Angeles (CZ 3B): a) All heatwaves detected and b) extreme heatwaves selection

619 For each city, the three extreme heatwaves (the most intense, most severe, and longest
620 heatwave) are selected.

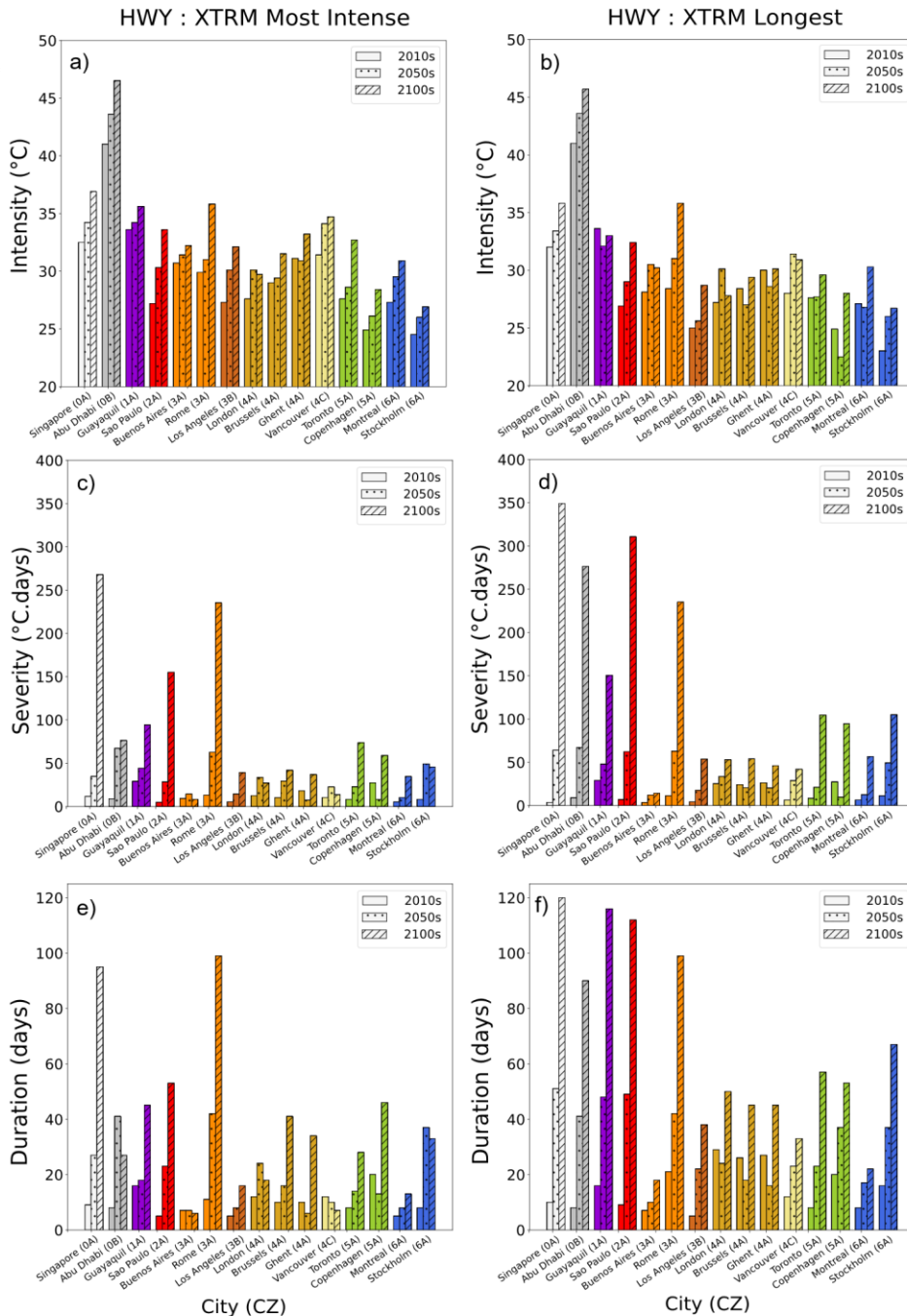


621
 622
 623
 624
 625
 626
 627
 628
 629
 630
 631

Figure 7 shows the characteristics (intensity, severity, and duration) of the most intense and longest heat waves in each climate zone. Characteristics of the most severe heatwaves are often similar to the longest heatwaves and are not shown here. The intensity of both extreme heatwaves strongly increases between the three periods and in each climate zone. The increase in intensity of the most intense heatwave by the end of the century is, in each city, between +2 °C (European cities in climate zone 4A) and +7 °C (Sao Paulo). The intensity of the longest heatwaves is between 0 °C and 3.4 °C (Vancouver), inferior to the most intense heatwaves in the 2010s, of 0 °C and 4.5 °C (Los Angeles) inferior in the 2050s, and of 0.2 and 3.8 °C (Vancouver) by the 2100s.

632

633 The extreme heatwaves' durations strongly increase between the three time periods,
634 especially the one of the longest heatwaves. The increase is more pronounced between 2100s
635 and 2050s than between 2050s and 2010s. By the 2010s, the duration of both the most intense
636 and longest extreme heat waves is generally around one to three weeks, depending on the
637 city. However, by 2050s, the extreme heatwaves last more than a month in Abu Dhabi (41
638 days), Rome (42 days), and Stockholm (37 days), between 6 and 24 days for the most intense
639 heatwaves in the other cities, between 7 and 49 days for the longest heatwaves in the other
640 cities. By the 2100s, in the five hottest cities (from climate zones 0A, 0B, 1A, 2A, and 3A), the
641 longest and the most intense heatwaves last 3 to 4 months. This high number is found because
642 the temperatures will constantly be above the current thresholds during the hot period of the
643 year. In other parts of the world, the longest heatwave will be between three weeks and 2
644 months long by the 2100s, except in Buenos Aires. For climate zone 3A, the severity and
645 duration of the heat waves in Rome are more significant than in Buenos Aires. This disparity
646 might be attributed to the heatwave data record, which shows European cities have more
647 exposure to heatwaves¹⁹. As expected, we observe that the durations of extreme intense
648 heatwaves are generally shorter than the longest heatwaves.

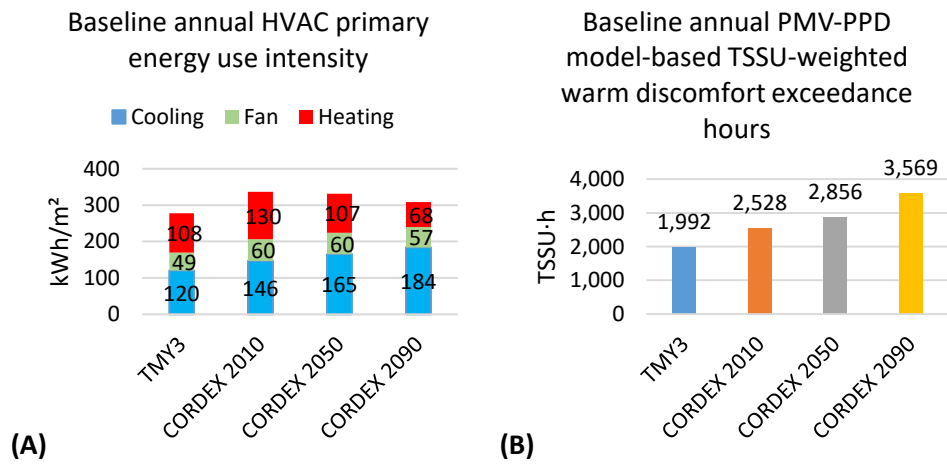


649
 650 *Figure 7 - Characteristics (intensity, severity, and duration) of the most intense and longest XTRM-HW: a) intensity*
 651 *of the most intense HW, b) intensity of the longest HW, c) severity of the most intense HW, d) severity of the longest*
 652 *HW, e) duration of the most intense HW, f) duration of the longest HW*

653 **Effect of future TMY and HWY weather files on building**
 654 **performance**

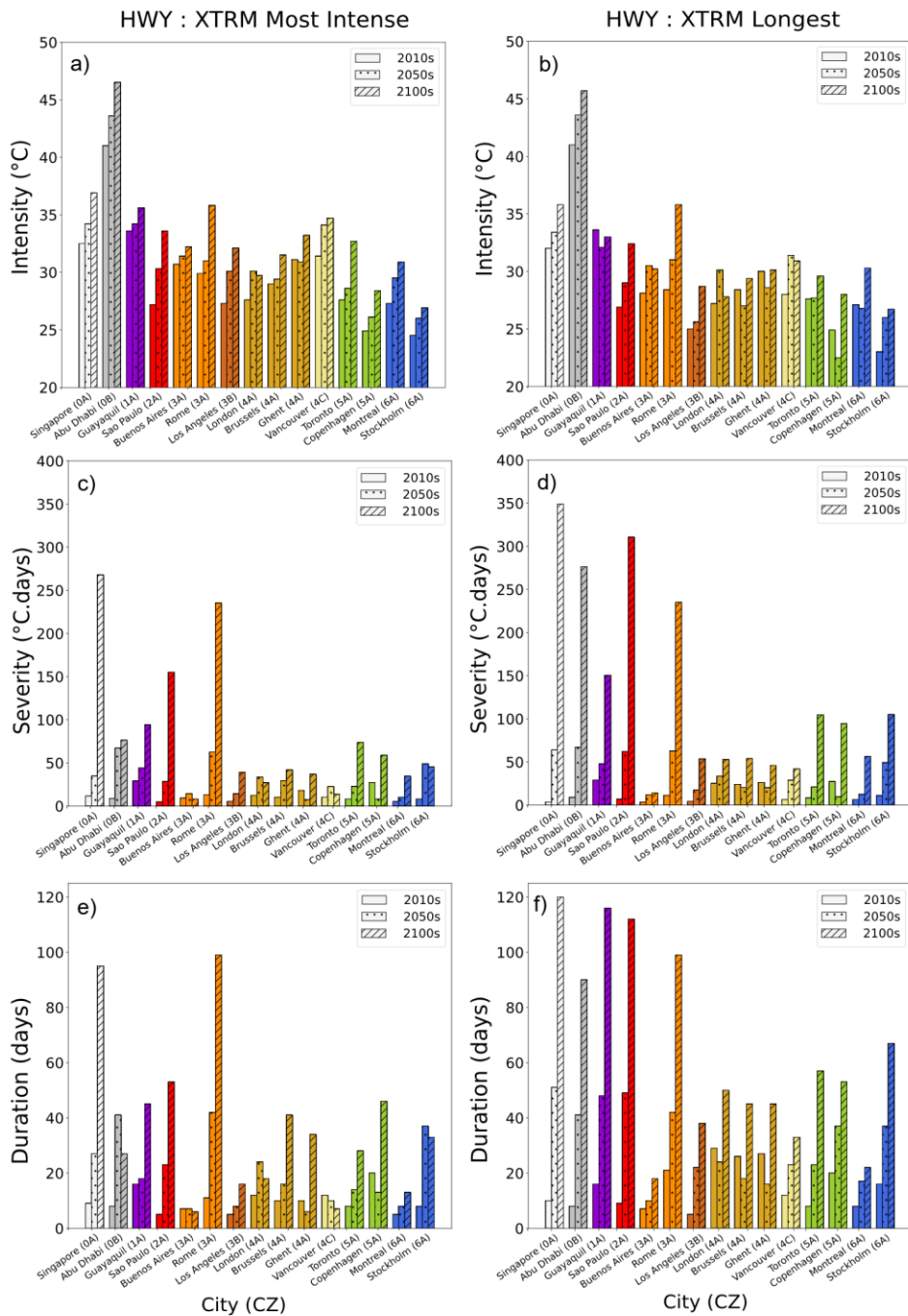
655
 656 Lee and Levinson⁶⁵ evaluated the effect of cool envelope strategies on heating, ventilation,
 657 and air conditioning (HVAC) primary energy use intensity and thermal comfort for a
 658 mechanically cooled single-family home in Los Angeles in Figure 8. They used the future TMYs

659 produced based on the methodology introduced in this paper (named CORDEX 2010, 2050,
 660 and 2090) as well as the historical Typical Meteorological Year 3 (TMY3), which spans 1991-
 661 2005⁶⁶. Panel A shows that cooling demand grows over time. They also calculated the thermal
 662 sensation scale unit (TSSU) weighted warm discomfort exceedance hours (TSSU·h) to evaluate
 663 the Predicted Mean Vote (PMV) based thermal comfort, which is the sum of summer thermal
 664 discomfort when PMV exceeds +0.7 according to ISO 1772-2:2018⁶⁷. PMV greater than +0.7 is
 665 considered uncomfortably warm during the summer season according to ISO 17772-1:2017
 666 Annex H.1 Category III⁶⁸. Annex H.1 Category III, considered uncomfortably warm during the
 667 summer season. Panel B shows that the occupants experience many more TSSU-weighted
 668 warm-discomfort exceedance hours in the future because the cooling system is sized based
 669 on historical TMY3 weather, which results in many hours during which the cooling system
 670 cannot meet future loads. They also show that use of passive strategies such as cool envelope
 671 materials, helps decrease these loads. These results emphasize the need to use future TMYs
 672 to anticipate an increase in cooling energy use intensity and take necessary action to adapt
 673 building design or refurbishment to future climate.
 674



675 **(A)**
 676 **(B)**
 677 *Figure 8 – Effect of future TMYs on energy use (A) and summer thermal discomfort (B) in an air-conditioned single-family home in Los Angeles (Lee and Levinson⁶⁵)*

678 Another example of how these weather files can be used is the work of Sengupta et al.⁶⁹ in
 679 which they evaluated the overheating of an educational building in Ghent, Belgium, under
 680 future weather files, comparing the results with the future TMY and HWY prepared in this
 681 paper. Educational buildings in Belgium are not equipped with mechanical air conditioning,
 682 and recent heat waves have already posed a threat to occupants' cognitive performance and
 683 health conditions. In their paper, they analyzed the thermal resilience of test lecture rooms
 684 with open windows at night for natural ventilation to flush heat and equipped with indirect
 685 evaporative cooling to cool the air during the daytime. Figure 9 shows the results of unmet
 686 degree hours (UDH) for different weather files: a) TMY and b) HWY (1A: 2010s intense HW,
 687 1B: 2010s severe and longest HW, 2A: 2050s intense HW, 2B: 2050s severe HW, 2C: 2050s
 688 longest HW, 3A: 2100s intense HW, 3B: 2100s severe and longest HW) with and without power
 689 outage (PO). The results emphasize that the HWYs present a much larger number of UDH when
 690 compared to TMY. The variety of HWY shows that HWY 1B leads to many UDHs due to its
 691 length of 28 days, while HWs of the 2100s also predict a very elevated number of UDHs due
 692 to the increase in outdoor temperatures



693 (

694 Figure 7). Additionally, a study by Sengupta et al.⁷⁰ identifying, quantifying, and comparing

695 different shocks that can increase overheating risk in buildings (e.g., outdoor shocks such as

696 heatwaves and mechanical shocks such as solar shading failure, cooling strategy failure,

697 natural night ventilation failure) proves that heatwaves are by far the most intense shocks for

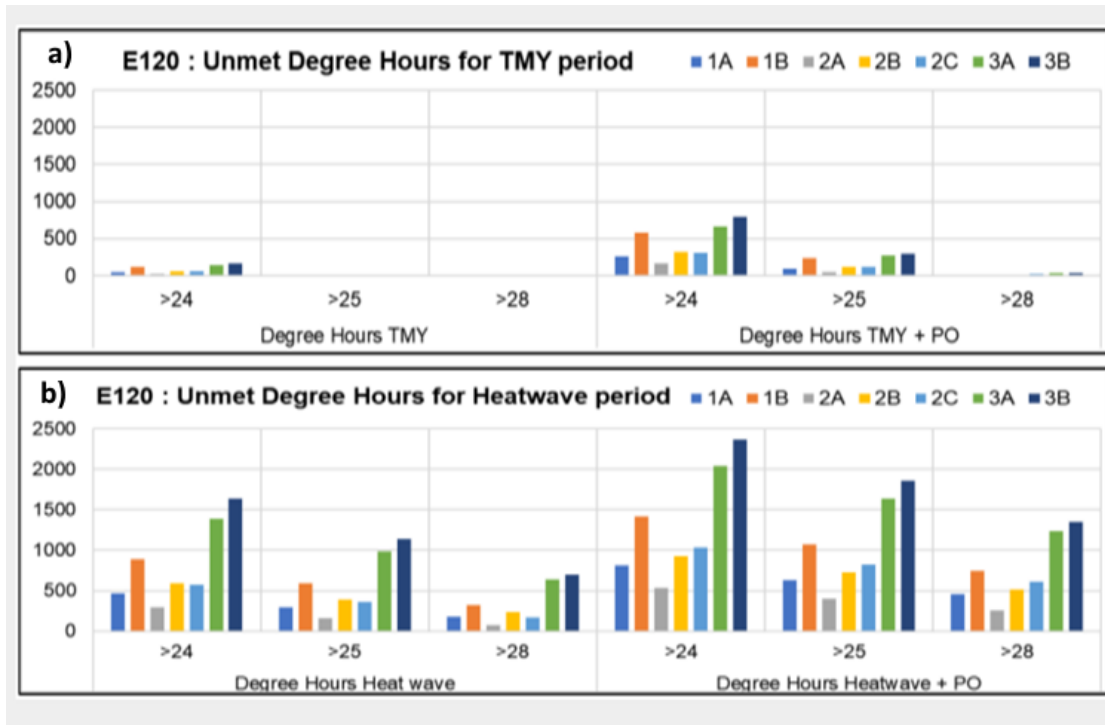
698 buildings that impact the thermal resilience to overheating. Thus, assessing and improving the

699 buildings' performance against heatwaves are a crucial step to future proof these buildings,

700 emphasizing the robust methodology needed to develop and utilize future weather data and

701 heatwave data to assess and design buildings.

702



704

705 *Figure 9 – a) Impact of future TMYs and b) Impact of future HWYs on summer thermal discomfort from Sengupta*
 706 *et al.*⁶⁹

707 Usage Notes

708 The provided typical meteorological years (TMY) and years containing heatwaves (HWY) in
 709 both EPW format are ready-to-use weather datasets to perform building performance
 710 simulations using Energy Plus, TRNSYS, or any other building energy model. They permit
 711 assessment of the thermal performance of buildings under typical and extreme future climate
 712 scenarios. Therefore, they help evaluate the efficiency and resilience of building renovation
 713 solutions to climate change in different climate zones. In particular, the TMY can be used to
 714 analyze changes in building heating and cooling loads under typical future weather conditions.
 715 The HWYs allow prediction of building thermal response under extreme heat events, which
 716 will be one major issue in the next decades. The multi-year (MY) datasets are also provided in
 717 CSV format to allow other authors to test different methods for assembling different types of
 718 future typical or extreme weather files for building performance assessments or in other
 719 sectors.

720

721 The provided datasets were generated based on the bias-corrected climate model MPI-ESM-
 722 LR/REMO, whose temperature projections are found to be the closest to the median of all
 723 climate model projections³¹. At least two other GCM/RCM model combinations satisfy the
 724 required spatial and temporal resolutions in the CORDEX database to generate weather files
 725 for building thermal performance analysis. These are the HadGEM2-ES/REMO and the
 726 NorESM1-M/REMO. Therefore, the results of this paper can be further expanded by
 727 comparing the outputs of all available CORDEX models. This can be used in future work to
 728 enrich the datasets. The datasets were generated based on RCP 8.5 climate projections, the
 729 worst-case socioeconomic scenario at the time of the IPCC AR5, and the most realistic based
 730 on the past and current emissions of greenhouse gases by the global community⁷¹. This means
 731 that they are suitable for applications in studies of system resilience, but they should be used
 732 with caution in building retrofits and HVAC system designs to avoid system oversizing or
 733 under-sizing.

734

735 It is possible to assemble additional weather files for other cities worldwide using other
736 climate models with the same methodology as provided in this paper. The Python code to
737 assemble the datasets from CORDEX climate projections is provided in the section “Code
738 Availability.” Additional weather variables, such as cloud cover, precipitation, and longwave
739 solar irradiance, would be an added value in the datasets. However, these additional variables
740 were not currently available for all cities, neither observation. Indeed, robust climate
741 observations are needed, and in this study, for some cities, only a few years (<10 years) of
742 observations for the bias correction were available, which can affect the final result to an
743 important extent for those cities. Future climate projections available on the CORDEX
744 platform, with the newest SSP scenarios from CMIP6, might allow the include additional
745 climate data in the datasets. In that case, observational data for these specific variables must
746 also be found to correct the model.

747

748 Given that the multi-year datasets are provided, they could be used to select heatwaves based
749 on methods different from the one chosen here. The common method used detects
750 heatwaves solely based on the temperature; however, in some hot and humid parts of the
751 world, humidity is known to be an important variable affecting indoor heat stress. The simple
752 method proposed here was validated for several cities in France and allows a standardized
753 approach that fits the purpose of a common method for all cities, climates, building typologies,
754 and other local specificities. Nevertheless, the multiyear datasets allow the use of additional
755 criteria to select the heatwaves with different methods. Beyond a different method, less
756 future extreme heatwaves could also be selected for building design⁴.

757

758 As explained in the “boundary conditions” section, the datasets do not incorporate urban
759 effects. In the selected GCM/RCM-REMO model, urban areas are represented as simple
760 impervious surfaces. Recent studies have shown that a more detailed urban parametrization
761 allows a better understanding of the regional-urban climate interactions and urban climate
762 effects, such as UHI intensity^{72–75}. However, this entails a significant increase in computing
763 power and time, limiting the analysis to shorter time periods. Due to such limitations in
764 modelling urban areas, the RCM REMO model does not accurately simulate climate
765 modifications induced by urban features, such as the urban heat island effect or urban
766 microclimates. Accordingly, bias-correction of the model projections was performed using
767 observational data from weather stations located outside cities. The urban heat island effect
768 and other urban climate modifications can be added to the weather datasets following
769 different methodologies already proposed in building performance simulation studies^{76–79}.
770 Most climate models do not explicitly model urban areas and, at best, describe them as rock
771 covers. Nonetheless, the very high resolutions reached now by the regional climate models
772 may justify and require a more realistic parameterization of surface exchanges between urban
773 canopy and atmosphere.

774

775 To quantify the potential impact of urbanization on the regional climate and evaluate the
776 benefits of a detailed urban canopy model compared with a simpler approach, a sensitivity
777 study was carried out over France at a 12km horizontal resolution with the ALADIN-Climate
778 regional model for 1980–2009 time period. Different descriptions of land use and urban
779 modeling were compared, corresponding to an explicit modeling of cities with the urban
780 canopy model TEB, a conventional and simpler approach representing urban areas as rocks,
781 and a vegetated experiment for which cities are replaced by natural covers. A general
782 evaluation of ALADIN-Climate was first done, which showed an overestimation of the incoming
783 solar irradiance but satisfying results in terms of precipitation and near-surface temperatures.
784 The sensitivity analysis then highlighted those urban areas had a significant impact on modeled
785 near-surface temperature. A further analysis of a few large French cities indicated that over

786 the 30 years of simulation, they all induced a warming effect both at daytime and nighttime
787 with values up to + 1.5 °C for the city of Paris. The urban model also led to regional warming
788 extending beyond the boundaries of urban areas. Finally, the comparison to temperature
789 observations available for the Paris area highlighted that the detailed urban canopy model
790 improved the modeling of the urban heat island compared with a simpler approach.
791 The urban heat island effect could be added to the weather datasets by using offline urban
792 canopy tools like the Urban Weather Generator (UWG)^{80,81}, the Surface Urban Energy and
793 Water Balance Scheme (SUEWS)⁸² module of the Urban Multi-scale Environmental
794 Predictor (UMEP) GIS tool, or other similar urban canopy models⁸³. Urban canopy models can
795 also be coupled with mesoscale models such as the Weather Research and Forecasting (WRF)
796 Model^{84,85} or the Global Environmental Multi-scale (GEM) Model⁸⁶ for a better consideration
797 of the urban boundary layer conditions⁸⁷. The UWG is an easy-to-use, computational
798 inexpensive tool that directly outputs urban weather files. However, it assumes that the city's
799 urban fabric is homogeneous and that the city is surrounded by rural areas. This can make its
800 results inaccurate for coastal cities or inhomogeneous urban fabrics^{88,89}. UWG accuracy may
801 also be limited by the simplified ways in which it calculates latent heat balance flux and urban
802 canyon wind speed⁸¹. Recently, new stand-alone UCM models have been developed that
803 overcome some of the UWG limitations, such as the Stand-alone Urban Energy/Climate Model
804 (SUECM)⁹⁰. City Fast Fluid Dynamics (CityFFD)⁹¹ and the Vertical-city Weather Generator
805 (VCWG)⁹². Machine learning techniques were also used to interpolate weather data spatially<sup>93-
806 95</sup>. Any of these tools can be used to add urban effects as well as the evolution of land use to
807 both the present and future TMYs and heatwave weather files presented in this data paper.

808 **Code Availability**

809 The source codes to generate these datasets from CORDEX climate data can be found at:
810 <https://zenodo.org/record/7300024#.ZBbi4XbMI2x>⁹⁶

811 **Acknowledgments**

812 The authors of the paper wish to thank their colleagues from IEA EBC Annex 80, who provided
813 insight and expertise during discussions on future weather data needed to assess resilient
814 cooling building design. The authors would like to acknowledge the World Climate Research
815 Programme's Working Group on Regional Climate and the Working Group on Coupled
816 Modelling, the former coordinating body of CORDEX and the responsible panel for CMIP5. We
817 also thank the climate modelling groups (listed in Table 2 of this paper) for producing and
818 making their model output available. We also acknowledge the Earth System Grid Federation
819 infrastructure, an international effort led by the U.S. Department of Energy's Program for
820 Climate Model Diagnosis and Intercomparison, the European Network for Earth System
821 Modelling, and other partners in the Global Organization for Earth System Science Portals (GO-
822 ESSP). Finally, the authors gratefully thank Alex J. Cannon for providing his code "Multivariate
823 Bias Correction of Climate Model Outputs". This work was partially supported by the Assistant
824 Secretary for Energy Efficiency and Renewable Energy, Building Technologies Office, of the
825 U.S. Department of Energy under Contract No. DE-AC02-05CH11231. Dr. Bre performed some
826 of the tasks regarding his contributions to this research during his OE-BUILDINGS action, under
827 grant agreement ID: 101024627. This project has received funding from the European Union's
828 Horizon 2020 research and innovation programme under the Marie Skłodowska-Curie grant
829 agreement N° 101024627. This research was supported, in part, by Fraunhofer Internal
830 Programs under Grant No. Attract 003-695033. The research was also partially supported by
831 Det Energiteknologisk Udviklingsog Demonstrations Program (EUDP) under grant 64018-0578.

832 **Author contributions**

833 Anaïs Machard, Agnese Salvati, Mamak P. Tootkaboni, and Abhishek Gaur coordinated the
834 efforts to produce these datasets, designed the methodology, and wrote and edited the draft.
835 All other authors prepared the datasets in the different cities and reviewed and edited the
836 manuscript.

837 **Competing interests**

838 The authors declare no competing interests.

839 **References**

- 840 1. Belcher, S., Hacker, J. & Powell, D. Constructing design weather data for future climates.
841 *Building Services Engineering Research and Technology* **26**, 49–61 (2005).
- 842 2. Nik, V. M. Making energy simulation easier for future climate – Synthesizing typical and
843 extreme weather data sets out of regional climate models (RCMs). *Applied Energy* **177**,
844 204–226 (2016).
- 845 3. Machard, A., Inard, C., Alessandrini, J.-M., Pelé, C. & Ribéron, J. A Methodology for
846 Assembling Future Weather Files Including Heatwaves for Building Thermal Simulations
847 from the European Coordinated Regional Downscaling Experiment (EURO-CORDEX)
848 Climate Data. *Energies* **13**, 3424 (2020).
- 849 4. Machard, A. Towards mitigation and adaptation to climate change: Contribution to
850 Building Design. (2021).
- 851 5. ISO. *ISO 15927-4:2005 Hygrothermal Performance of Buildings — Calculation and*
852 *Presentation of Climatic Data — Part 4: Hourly Data for Assessing the Annual Energy Use*
853 *for Heating and Cooling*. (2005).
- 854 6. Ouzeau, G., Soubeyroux, J.-M., Schneider, M., Vautard, R. & Planton, S. Heat waves
855 analysis over France in present and future climate: Application of a new method on the
856 EURO-CORDEX ensemble. *Climate Services* **4**, 1–12 (2016).
- 857 7. Doutreloup, S. *et al.* Historical and future weather data for dynamic building simulations
858 in Belgium using the regional climate model MAR: typical and extreme meteorological
859 year and heatwaves. *Earth Syst. Sci. Data* **14**, 3039–3051 (2022).

- 860 8. Ramon, D., Allacker, K., van Lipzig, N. P. M., De Troyer, F. & Wouters, H. Future Weather
861 Data for Dynamic Building Energy Simulations: Overview of Available Data and
862 Presentation of Newly Derived Data for Belgium. in *Energy Sustainability in Built and*
863 *Urban Environments* (eds. Motoasca, E., Agarwal, A. K. & Breesch, H.) 111–138 (Springer
864 Singapore, Singapore, 2019). doi:10.1007/978-981-13-3284-5_6.
- 865 9. Ramon, D., Allacker, K., Trigaux, D., Wouters, H. & Van Lipzig, N. P. M. Dynamic modelling
866 of operational energy use in a building LCA: A case study of a Belgian office building.
867 *Energy and Buildings* **278**, 112634 (2023).
- 868 10. Ramon, D., Allacker, K., De Troyer, F., Wouters, H. & Van Lipzig, N. P. M. Future heating
869 and cooling degree days for Belgium under a high-end climate change scenario. *Energy*
870 *and Buildings* **216**, 109935 (2020).
- 871 11. Gaur, A. & Lacasse, M. Climate Data to Support the Adaptation of Buildings to Climate
872 Change in Canada. *Data* **7**, 42 (2022).
- 873 12. Zou, J., Gaur, A., Wang, L. (Leon), Laouadi, A. & Lacasse, M. Assessment of future
874 overheating conditions in Canadian cities using a reference year selection method.
875 *Building and Environment* **218**, 109102 (2022).
- 876 13. Bass, B., New, J., Rastogi, D. & Kao, S.-C. Future Typical Meteorological Year (fTMY) US
877 Weather Files for Building Simulation. <https://zenodo.org/record/6939750> (2022).
- 878 14. ASHRAE. *ANSI/ASHRAE Standard 169-2013, Climatic Data for Building Design*. (ASHRAE,
879 Atlanta, 2013).
- 880 15. Holzer, P. & Cooper, P. *IEA EBC Annex 80 on Resilient Cooling for Residential and Small*
881 *Non-Residential Buildings*. 14 [https://annex80.iea-](https://annex80.iea-ebc.org/Data/Sites/10/media/documents/supporting/ebc-annex-80-annex-text-190616.pdf)
882 [ebc.org/Data/Sites/10/media/documents/supporting/ebc-annex-80-annex-text-](https://annex80.iea-ebc.org/Data/Sites/10/media/documents/supporting/ebc-annex-80-annex-text-190616.pdf)
883 [190616.pdf](https://annex80.iea-ebc.org/Data/Sites/10/media/documents/supporting/ebc-annex-80-annex-text-190616.pdf) (2019).
- 884 16. Attia, S. *et al. Framework to Evaluate the Resilience of Different Cooling Technologies*.
885 (2021). doi:10.13140/RG.2.2.33998.59208.

- 886 17. Rahif, R. *et al.* Simulation-based framework to evaluate resistivity of cooling strategies in
887 buildings against overheating impact of climate change. *Building and Environment* **208**,
888 108599 (2022).
- 889 18. Li, D. H. W., Yang, L. & Lam, J. C. Impact of climate change on energy use in the built
890 environment in different climate zones – A review. *Energy* **42**, 103–112 (2012).
- 891 19. Centre for Research on the Epidemiology of Disasters - CRED, Ucl., Brussels, Belgium. EM-
892 DAT. <https://www.emdat.be/>.
- 893 20. United Nations, Department of Economic and Social Affairs, Population Division (2022).
894 2022 Revision of World Population Prospects. <https://population.un.org/wpp/>.
- 895 21. Machard, A. *et al.* Climate change influence on buildings dynamic thermal behavior during
896 summer overheating periods: An in-depth sensitivity analysis. *Energy and Buildings* **284**,
897 112758 (2023).
- 898 22. Giorgi, F. *et al.* The CORDEX-CORE EXP-I Initiative: Description and Highlight Results from
899 the Initial Analysis. *Bulletin of the American Meteorological Society* **103**, E293–E310
900 (2022).
- 901 23. Teichmann, C. *et al.* Assessing mean climate change signals in the global CORDEX-CORE
902 ensemble. *Clim Dyn* **57**, 1269–1292 (2021).
- 903 24. Taylor, K. E., Stouffer, R. J. & Meehl, G. A. An Overview of CMIP5 and the Experiment
904 Design. *Bulletin of the American Meteorological Society* **93**, 485–498 (2012).
- 905 25. Eyring, V. *et al.* Overview of the Coupled Model Intercomparison Project Phase 6 (CMIP6)
906 experimental design and organization. *Geosci. Model Dev.* **9**, 1937–1958 (2016).
- 907 26. Van Vuuren, D. P. *et al.* The representative concentration pathways: an overview. *Climatic*
908 *Change* **109**, 5–31 (2011).
- 909 27. Riahi, K. *et al.* RCP 8.5—A scenario of comparatively high greenhouse gas emissions.
910 *Climatic Change* **109**, 33–57 (2011).

- 911 28. Cannon, A. J. & Jeong, D. I. *Climate-Resilient Buildings and Core Public Infrastructure 2020:*
912 *An Assessment of the Impact of Climate Change on Climatic Design Data in Canada.*
913 (Environment and Climate Change Canada, Gatineau, QC, CA, 2021).
- 914 29. McSweeney, C. F., Jones, R. G., Lee, R. W. & Rowell, D. P. Selecting CMIP5 GCMs for
915 downscaling over multiple regions. *Clim Dyn* **44**, 3237–3260 (2015).
- 916 30. World Climate Research Program, C. R. C. D. E. CORDEX CORE Simulations CORDEX
917 Coordinated Output for Regional Evaluations (CORE). [https://cordex.org/experiment-](https://cordex.org/experiment-guidelines/cordex-core/cordex-core-simulations/)
918 [guidelines/cordex-core/cordex-core-simulations/](https://cordex.org/experiment-guidelines/cordex-core/cordex-core-simulations/).
- 919 31. Flato, G. *et al.* Evaluation of Climate Models. In: *Climate Change 2013: The Physical Science*
920 *Basis. Contribution of Working Group I to the Fifth Assessment Report of the*
921 *Intergovernmental Panel on Climate Change.* (2013).
- 922 32. Giorgetta, M. A. *et al.* Climate and carbon cycle changes from 1850 to 2100 in MPI-ESM
923 simulations for the Coupled Model Intercomparison Project phase 5: Climate Changes in
924 MPI-ESM. *J. Adv. Model. Earth Syst.* **5**, 572–597 (2013).
- 925 33. Jacob, D. & Podzun, R. Sensitivity studies with the regional climate model REMO. *Meteorol.*
926 *Atmos. Phys.* **63**, 119–129 (1997).
- 927 34. Jacob, D. A note to the simulation of the annual and inter-annual variability of the water
928 budget over the Baltic Sea drainage basin. *Meteorology and Atmospheric Physics* **77**, 61–
929 73 (2001).
- 930 35. Roeckner, E. *et al.* *THE ATMOSPHERIC GENERAL CIRCULATION MODEL ECHAM-4: MODEL*
931 *DESCRIPTION AND SIMULATION OF PRESENT-DAY CLIMATE.* (1996).
- 932 36. Hagemann, S. *An Improved Land Surface Parameter Dataset for Global and Regional*
933 *Climate Models.* (2002).
- 934 37. Pfeifer, S. Modeling cold cloud processes with the regional climate model REMO. (Max
935 Planck Institute, Hamburg, 2006).

- 936 38. Kotlarski, S. A Subgrid Glacier Parameterisation for Use in Regional Climate Modelling.
937 (Max Planck Institute, Hamburg, 2007).
- 938 39. Teichmann, C. Climate and Air Pollution Modelling in South America with Focus on
939 Megacities. (Max Planck Institute, Hamburg, 2010).
- 940 40. Semmler, T., Cheng, B., Yang, Y. & Rontu, L. Snow and ice on Bear Lake (Alaska) – sensitivity
941 experiments with two lake ice models. *Tellus A: Dynamic Meteorology and Oceanography*
942 **64**, 17339 (2012).
- 943 41. Pietikäinen, J.-P. *et al.* The regional aerosol-climate model REMO-HAM. *Geosci. Model*
944 *Dev.* **5**, 1323–1339 (2012).
- 945 42. Preuschmann, S. Regional surface albedo characteristics - analysis of albedo data and
946 application to land-cover changes for a regional climate model. (Max Planck Institute,
947 Hamburg, 2012).
- 948 43. Wilhelm, C., Rechid, D. & Jacob, D. Interactive coupling of regional atmosphere with
949 biosphere in the new generation regional climate system model REMO-iMOVE. *Geosci.*
950 *Model Dev.* **7**, 1093–1114 (2014).
- 951 44. Maraun, D. Bias Correcting Climate Change Simulations - a Critical Review. *Curr Clim*
952 *Change Rep* **2**, 211–220 (2016).
- 953 45. Faghieh, M., Brissette, F. & Sabeti, P. *Impact of Correcting Sub-Daily Climate Model Biases*
954 *for Hydrological Studies*. [https://hess.copernicus.org/preprints/hess-2021-236/hess-](https://hess.copernicus.org/preprints/hess-2021-236/hess-2021-236.pdf)
955 [2021-236.pdf](https://hess.copernicus.org/preprints/hess-2021-236/hess-2021-236.pdf) (2021) doi:10.5194/hess-2021-236.
- 956 46. Yang, W., Gardelin, M., Olsson, J. & Bosshard, T. Multi-variable bias correction: application
957 of forest fire risk in present and future climate in Sweden. *Nat. Hazards Earth Syst. Sci.* **15**,
958 2037–2057 (2015).
- 959 47. Gaur, A., Lacasse, M. & Armstrong, M. Climate Data to Undertake Hygrothermal and
960 Whole Building Simulations Under Projected Climate Change Influences for 11 Canadian
961 Cities. *Data* **4**, 72 (2019).

- 962 48. Cannon, A. J. Multivariate quantile mapping bias correction: an N-dimensional probability
963 density function transform for climate model simulations of multiple variables. *Clim Dyn*
964 **50**, 31–49 (2018).
- 965 49. Cannon, A. J., Sobie, S. R. & Murdock, T. Q. Bias Correction of GCM Precipitation by
966 Quantile Mapping: How Well Do Methods Preserve Changes in Quantiles and Extremes?
967 *Journal of Climate* **28**, 6938–6959 (2015).
- 968 50. Qingyuan, Z., Huang, J. & Siwei, L. DEVELOPMENT OF TYPICAL YEAR WEATHER DATA FOR
969 CHINESE LOCATIONS. *ASHRAE Transactions* 2002, v. 108. Pt. 2, held June 2002, Honolulu,
970 Hawaii.
- 971 51. Boland, J., Ridley, B. & Brown, B. Models of diffuse solar radiation. *Renewable Energy* **33**,
972 575–584 (2008).
- 973 52. UNI. *UNI 10349-1:2016 Heating and Cooling of Buildings-Climatic Data-Part 1: Monthly*
974 *Means for Evaluation of Energy Need for Space Heating and Cooling and Methods for*
975 *Splitting Global Solar Irradiance into the Direct and Diffuse Parts and to Calculate the Solar*
976 *Irradiance on Tilted Planes.* (2016).
- 977 53. Ridley, B., Boland, J. & Lauret, P. Modelling of diffuse solar fraction with multiple
978 predictors. *Renewable Energy* **35**, 478–483 (2010).
- 979 54. Kasten, F. THE LINKE TURBIDITY FACTOR BASED ON IMPROVED VALUES OF THE INTEGRAL
980 RAYLEIGH OPTICAL THICKNESS. *Solar Energy* **56**, 6 (1996).
- 981 55. Remund, J., Wald, L., Lefèvre, M., Ranchin, T. & Page, J. Worldwide Linke turbidity
982 information. *ISES Solar World Congress* 14.
- 983 56. Remund, J. & Domeisen, D. Aerosol Optical Depth and Linke Turbidity Climatology:
984 Description for Final Report of IEA SHC Task 36. *Meteotest, Bern, Switzerland* (2009).
- 985 57. Finkelstein, J. M. & Schafer, R. E. Improved goodness-of-fit tests. *Biometrika* **58**, 6 (1971).
- 986 58. U.S. Department of Energy. EnergyPlus™ Version 9.6.0 Documentation/Auxiliary
987 Programs. **Chapter 2**, 257 (2021).

- 988 59. Flores-Larsen, S., Bre, F. & Hongn, M. A performance-based method to detect and
989 characterize heatwaves for building resilience analysis. *Renewable and Sustainable Energy*
990 *Reviews* **167**, 112795 (2022).
- 991 60. Machard, A. *et al.* IEA EBC Annex 80 'Typical and extreme weather datasets for studying
992 the resilience of buildings to climate change' (Version 1.0). 2024-02-26
993 https://doi.org/10.26050/WDCC/WDTF_Annex80_build_v1.0 (2024).
- 994 61. Meteotest. Meteonorm Software. <https://meteonorm.meteotest.ch/en/>.
- 995 62. IEA EBC Annex 80 - Resilient Cooling of Buildings. Weather Data.
- 996 63. Ohunakin, O. S., Adaramola, M. S., Oyewola, O. M., Matthew, O. J. & Fagbenle, R. O. The
997 effect of climate change on solar radiation in Nigeria. *Solar Energy* **116**, 272–286 (2015).
- 998 64. Cutforth, H. W. & Judiesch, D. Long-term changes to incoming solar energy on the
999 Canadian Prairie. *Agricultural and Forest Meteorology* **145**, 167–175 (2007).
- 1000 65. Lee, S. H. & Levinson, R. Cool envelope benefits in future typical weather and heatwave
1001 conditions 1 for single-family homes in Los Angeles [accepted paper]. *Sixth International*
1002 *Conference on Countermeasures to Urban Heat Islands, RMIT University, Melbourne,*
1003 *Australia.* (2023) doi:10.20357/B7DK6T.
- 1004 66. Wilcox, S. & Marion, W. Users Manual for TMY3 Data Sets. *Technical Report (NREL/TP-*
1005 **581-43156). National Renewable Energy Lab.,** (2008).
- 1006 67. ISO. ISO/TR 17772-2:2018 Energy performance of buildings — Overall energy
1007 performance assessment procedures — Part 2: Guideline for using indoor environmental
1008 input parameters for the design and assessment of energy performance of buildings.
1009 (2018).
- 1010 68. ISO. ISO 17772-1:2017 Energy performance of buildings — Indoor environmental quality
1011 — Part 1: Indoor environmental input parameters for the design and assessment of energy
1012 performance of buildings. (2017).

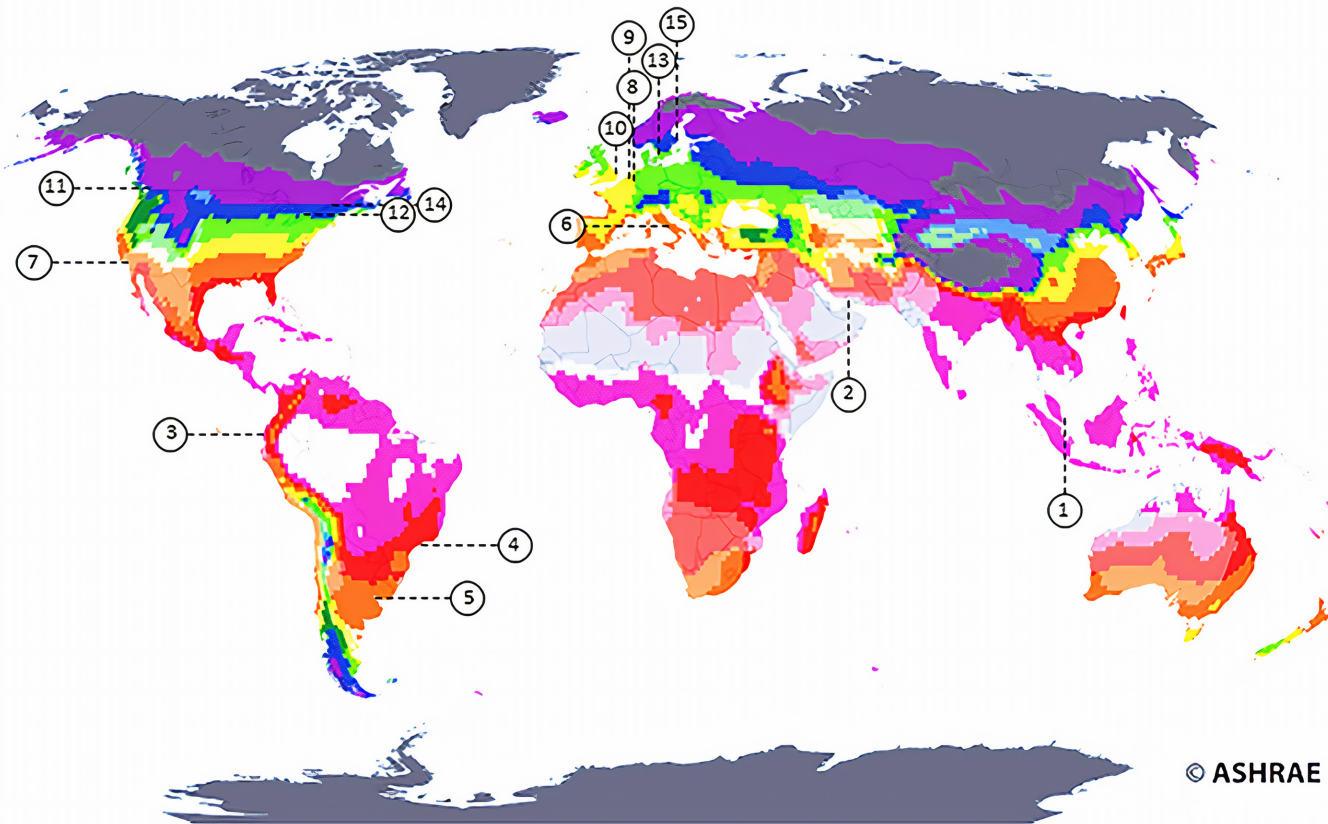
- 1013 69. Sengupta, A., Breesch, H., Al Assaad, D. & Steeman, M. Evaluation of thermal resilience to
1014 overheating for an educational building in future heatwave scenarios. *International*
1015 *Journal of Ventilation* 1–11 (2023) doi:10.1080/14733315.2023.2218424.
- 1016 70. Sengupta, A., Al Assaad, D., Bastero, J. B., Steeman, M. & Breesch, H. Impact of heatwaves
1017 and system shocks on a nearly zero energy educational building: Is it resilient to
1018 overheating? *Building and Environment* **234**, 110152 (2023).
- 1019 71. Schwalm, C. R., Glendon, S. & Duffy, P. B. RCP8.5 tracks cumulative CO2 emissions. in
1020 *Proceedings of the National Academy of Sciences* vol. 117 19656–19657 (2020).
- 1021 72. Daniel, M. *et al.* Benefits of explicit urban parameterization in regional climate modeling
1022 to study climate and city interactions. *Clim Dyn* **52**, 2745–2764 (2019).
- 1023 73. Langendijk, G. S., Rechid, D., Sieck, K. & Jacob, D. Added value of convection-permitting
1024 simulations for understanding future urban humidity extremes: case studies for Berlin and
1025 its surroundings. *Weather and Climate Extremes* **33**, 100367 (2021).
- 1026 74. Trusilova, K. *et al.* The urban land use in the COSMO-CLM model: a comparison of three
1027 parameterizations for Berlin. *metz* **25**, 231–244 (2016).
- 1028 75. Gao, Y. *et al.* Implementation of the CORINE land use classification in the regional climate
1029 model REMO. **20**, (2020).
- 1030 76. Taha, H. SITE-SPECIFIC WEATHER FILES AND FINE-SCALE PROBABILISTIC MICROCLIMATE
1031 ZONES FOR CURRENT AND FUTURE CLIMATES AND LAND USE. *IBPSA World News* 29–41
1032 (2020).
- 1033 77. Salvati, A., Palme, M., Chiesa, G. & Kolokotroni, M. Built form, urban climate and building
1034 energy modelling: case-studies in Rome and Antofagasta. *Journal of Building Performance*
1035 *Simulation* **13**, 209–225 (2020).
- 1036 78. Masson, V., Lemonsu, A., Hidalgo, J. & Voogt, J. Urban Climates and Climate Change. *Annu.*
1037 *Rev. Environ. Resour.* **45**, 411–444 (2020).

- 1038 79. Salvati, A. & Kolokotroni, M. Generating future-urban weather files for building
1039 performance simulations: case studies in London. in *Proceedings of the 17th IBPSA*
1040 *Conference* (Bruges, Belgium, 2021). doi:10.26868/25222708.2021.30315.
- 1041 80. Bueno, B., Norford, L., Hidalgo, J. & Pigeon, G. The urban weather generator. *Journal of*
1042 *Building Performance Simulation* **6**, 269–281 (2013).
- 1043 81. Mao, J., Yang, J. H., Afshari, A. & Norford, L. K. Global sensitivity analysis of an urban
1044 microclimate system under uncertainty: Design and case study. *Building and Environment*
1045 **124**, 153–170 (2017).
- 1046 82. Ward, H. C., Kotthaus, S., Järvi, L. & Grimmond, C. S. B. Surface Urban Energy and Water
1047 Balance Scheme (SUEWS): Development and evaluation at two UK sites. *Urban Climate*
1048 **18**, 1–32 (2016).
- 1049 83. Leroyer, S., Bélair, S., Spacek, L. & Gultepe, I. Modelling of radiation-based thermal stress
1050 indicators for urban numerical weather prediction. *Urban Climate* **25**, 64–81 (2018).
- 1051 84. Skamarock, W. C. *et al.* A Description of the Advanced Research WRF Model Version 4.
1052 165.
- 1053 85. Chen, F. *et al.* The Integrated WRF/Urban Modeling System: Development, Evaluation,
1054 and Applications to Urban Environmental Problems. 40.
- 1055 86. Yeh, K.-S. *et al.* The CMC–MRB Global Environmental Multiscale (GEM) Model. Part III:
1056 Nonhydrostatic Formulation. *Mon. Wea. Rev.* **130**, 339–356 (2002).
- 1057 87. Shu, C. *et al.* Added value of convection permitting climate modelling in urban overheating
1058 assessments. *Building and Environment* **207**, 108415 (2022).
- 1059 88. Martinez, S. *et al.* A practical approach to the evaluation of local urban overheating– A
1060 coastal city case-study. *Energy and Buildings* **253**, 111522 (2021).
- 1061 89. Salvati, A., Monti, P., Coch Roura, H. & Cecere, C. Climatic performance of urban textures:
1062 Analysis tools for a Mediterranean urban context. *Energy and Buildings* **185**, 162–179
1063 (2019).

- 1064 90. Afshari, A. & Ramirez, N. Improving the accuracy of simplified urban canopy models for
1065 arid regions using site-specific prior information. *Urban Climate* **35**, 100722 (2021).
- 1066 91. Mortezaazadeh, M., Wang, L. L., Albettar, M. & Yang, S. CityFFD – City fast fluid dynamics
1067 for urban microclimate simulations on graphics processing units. *Urban Climate* **41**,
1068 101063 (2022).
- 1069 92. Moradi, M., Krayenhoff, E. S. & Aliabadi, A. A. A comprehensive indoor–outdoor urban
1070 climate model with hydrology: The Vertical City Weather Generator (VCWG v2.0.0).
1071 *Building and Environment* **207**, 108406 (2022).
- 1072 93. Gaur, A., Eichenbaum, M. K. & Simonovic, S. P. Analysis and modelling of surface Urban
1073 Heat Island in 20 Canadian cities under climate and land-cover change. *Journal of*
1074 *Environmental Management* **206**, 145–157 (2018).
- 1075 94. Leirvik, T. & Yuan, M. A Machine Learning Technique for Spatial Interpolation of Solar
1076 Radiation Observations. *Earth and Space Science* **8**, (2021).
- 1077 95. Appelhans, T., Mwangomo, E., Hardy, D. R., Hemp, A. & Nauss, T. Evaluating machine
1078 learning approaches for the interpolation of monthly air temperature at Mt. Kilimanjaro,
1079 Tanzania. *Spatial Statistics* **14**, 91–113 (2015).
- 1080 96. Machard, A. AMachard/Assembling-future-weather-files-including-heatwaves: v1.0.0
1081 (v1.0.0). Zenodo. <https://doi.org/10.5281/zenodo.7300024> (2022).

1082
1083

CZ	Description
0A	Extremely Hot Humid
0B	Extremely Hot Dry
1A	Very Hot Humid
1B	Very Hot Dry
2A	Hot Humid
2B	Hot Dry
3A	Warm Humid
3B	Warm Dry
3C	Warm Marine
4A	Mixed Humid
4B	Mixed Dry
4C	Mixed Marine
5A	Cool Humid
5B	Cool Dry
5C	Cool Marine
6A	Cold Humid
6B	Cold Dry
7	Very Cold
8	Subarctic / Arctic



- 1 Singapore
- 2 Abu Dhabi
- 3 Guayaquil
- 4 São Paulo
- 5 Buenos Aires
- 6 Rome
- 7 Los Angeles
- 8 Brussels
- 9 Ghent
- 10 London
- 11 Vancouver
- 12 Toronto
- 13 Copenhagen
- 14 Montreal
- 15 Stockholm

© ASHRAE

Source data:

- 1) **Regional Climate Model data (CORDEX)**
Periods: 2001-2020, 2041-2060, 2081-2100
- +
- 2) **Hourly historical observations**
5-20 years, depending on city

Step 1

- 1) **Extraction of CORDEX data**
To extract climate data from NetCDF files.
Method: Python code (Machard et al., 2020) OR NetCDF extractor
- 2) **Interpolation CORDEX data**
to transform 3hrs to 1hr frequency data, if needed

Outputs: Hourly weather datasets for the three 20-years periods in .csv format

Step 2

- 1) **Bias-adjustment of CORDEX data**
To correct the bias associated to simulated RCM data using observations. **Method:** Multivariate Bias Correction (Cannon, 2018)
- 2) **Splitting global solar radiation**
To estimate direct normal and diffuse radiation from global horizontal radiation. **Method:** Bolan-Ridley model (Boland et al., 2008)

Outputs: Bias-adjusted Hourly weather datasets for the three 20-years periods in .csv format

Step 3

- 1) **Typical Meteorological Years (TMYs)**
Selection of appropriate meteorological data from 20 years bias-adjusted hourly data.
Method: EN ISO 15927-4:2005 standard
- 2) **Detect and characterize heatwaves**
across the hourly bias-adjusted datasets
Method: Ouzeau et al. 2016
- 3) **Select extreme heatwaves**

Final Outputs

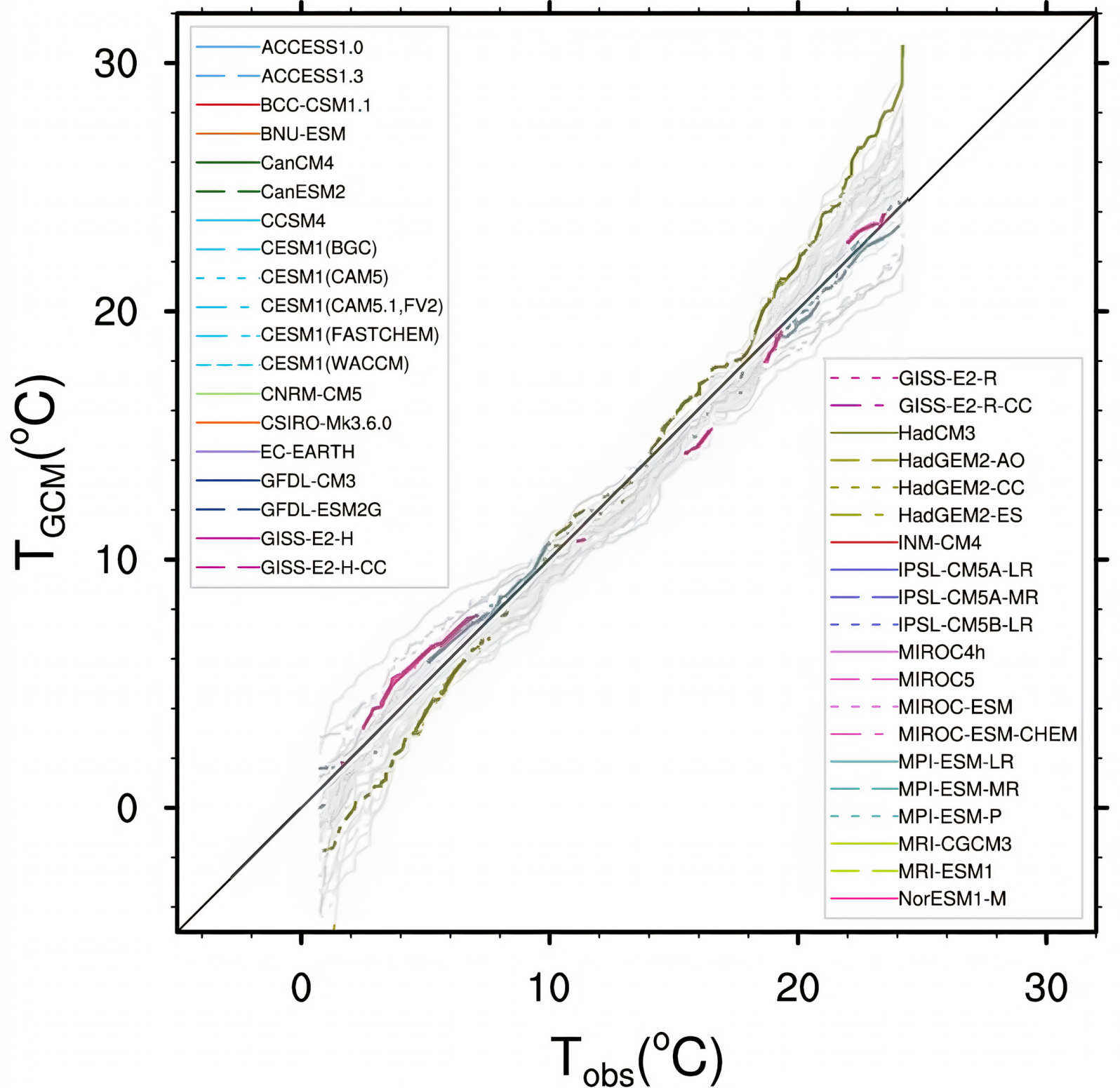
Typical meteorological years (.epw)

- Historical (~2010)
- Future : medium term (~2050)
- Future: long term (~2090)

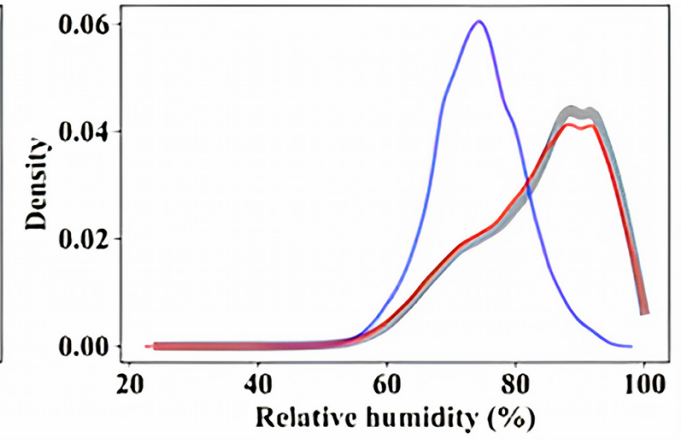
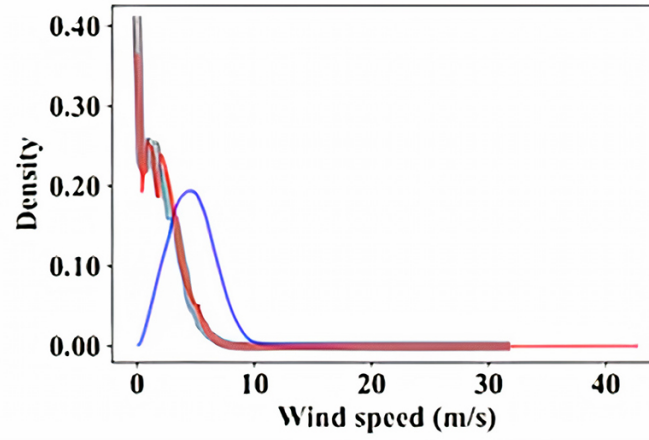
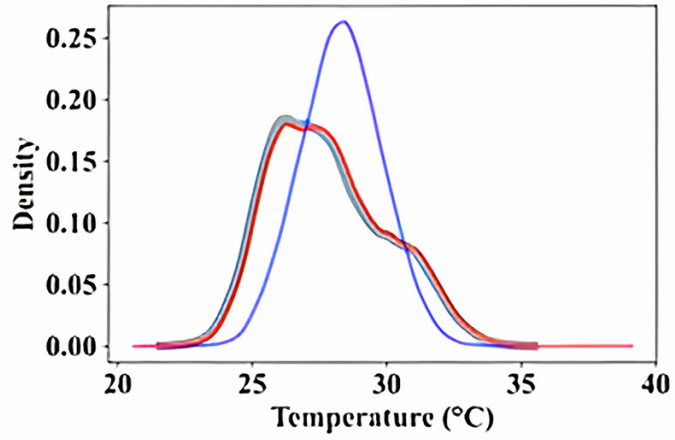
Extreme heatwave years (.epw)

- Historical (~2010)
- Future : medium term (~2050)
- Future: long term (~2090)

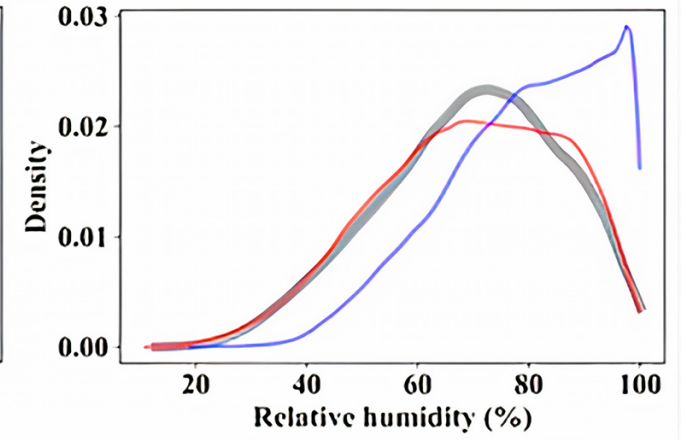
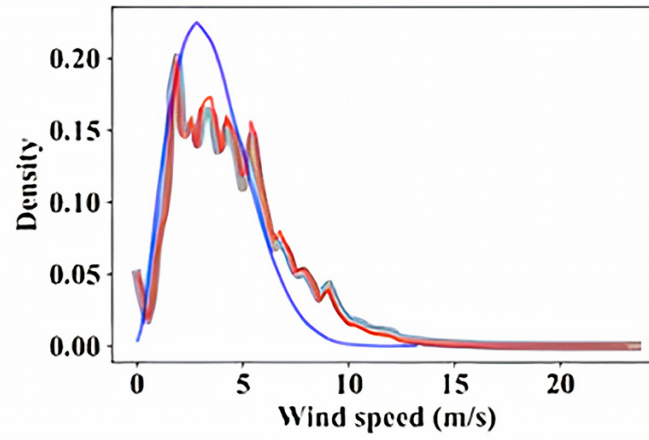
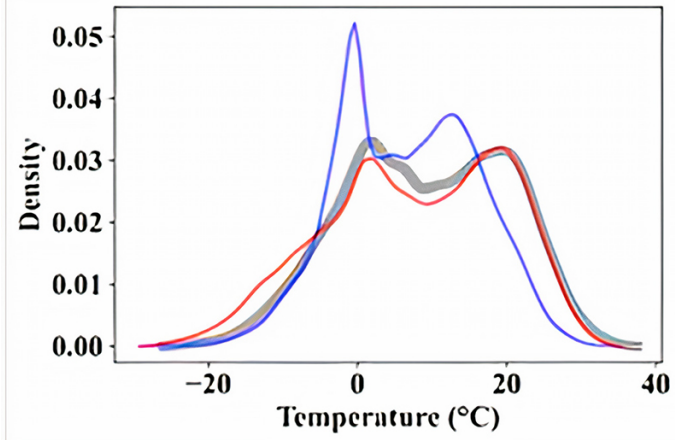
(b) CMIP5 (color) & CMIP3 (grey)



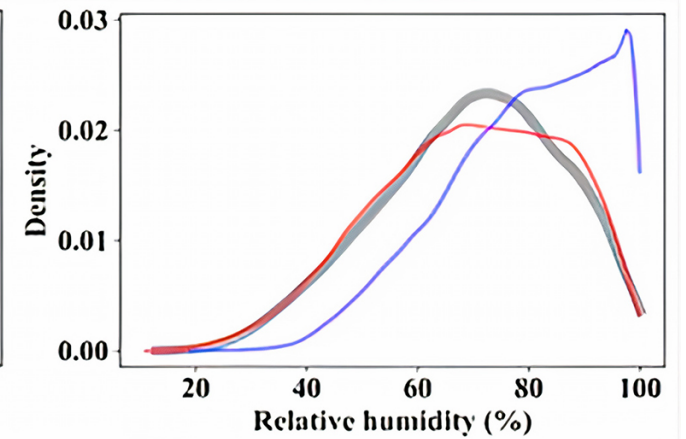
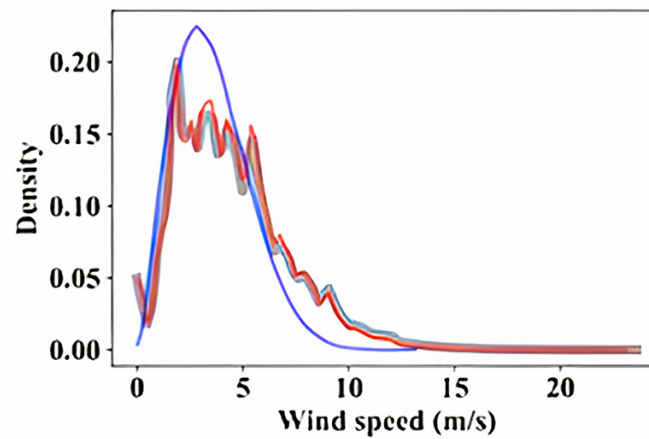
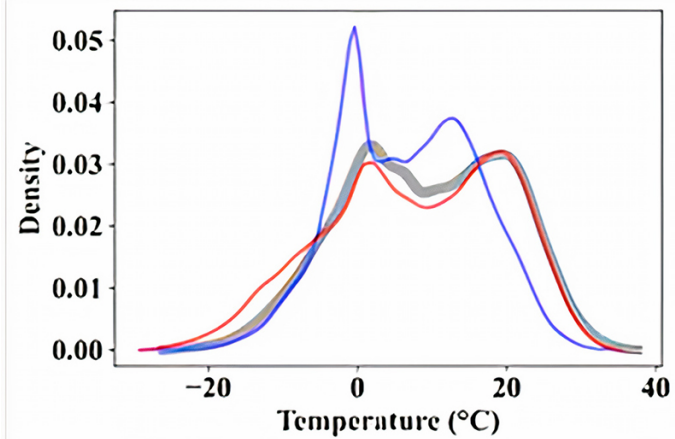
Singapore

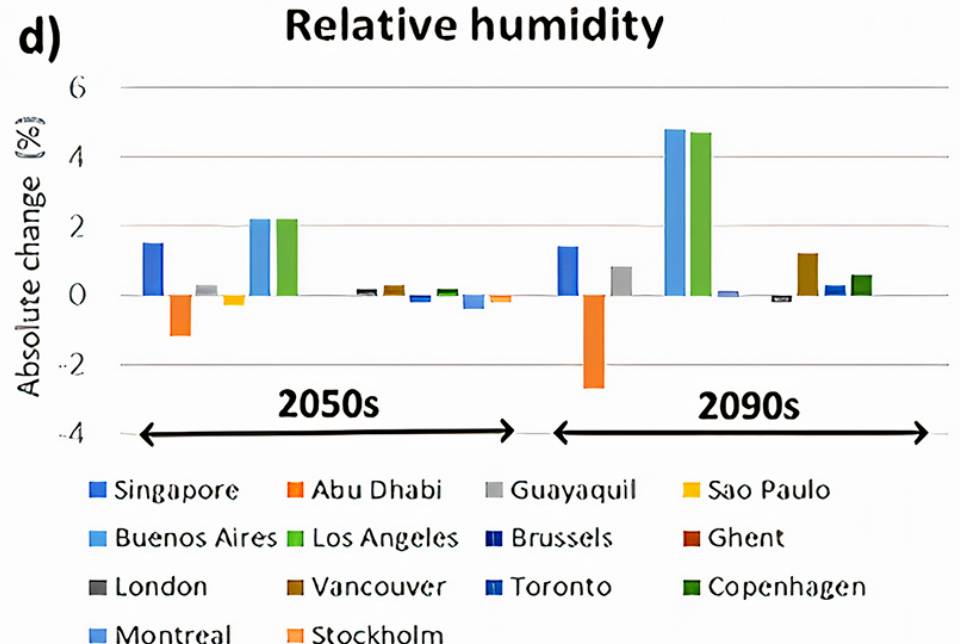
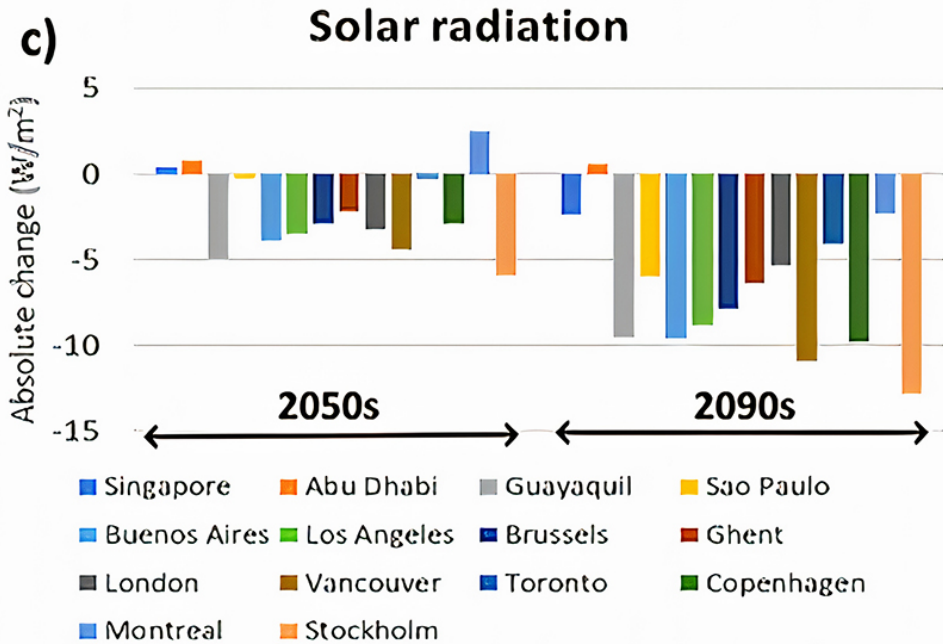
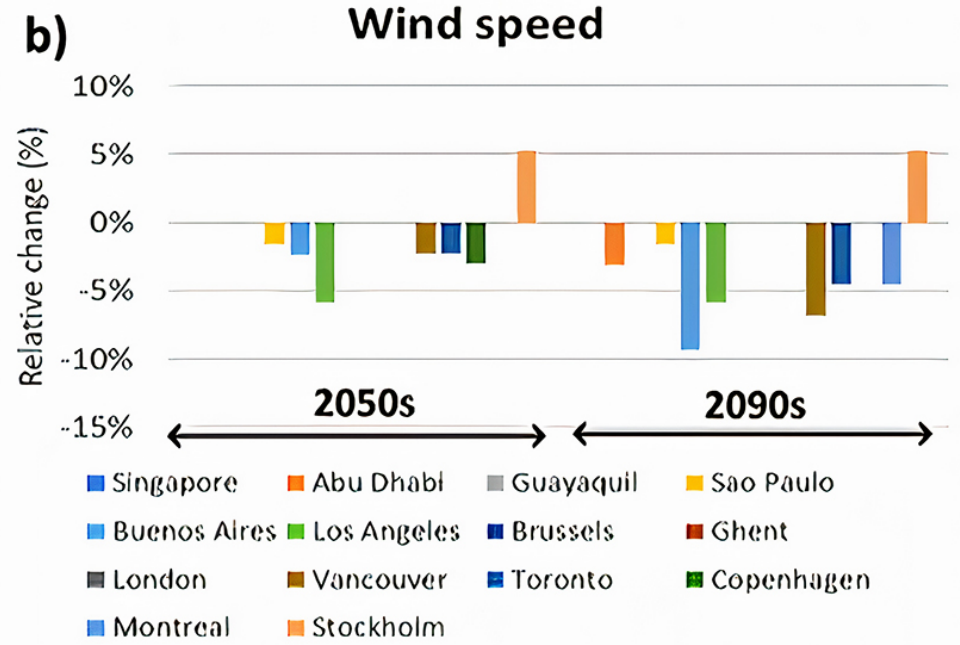
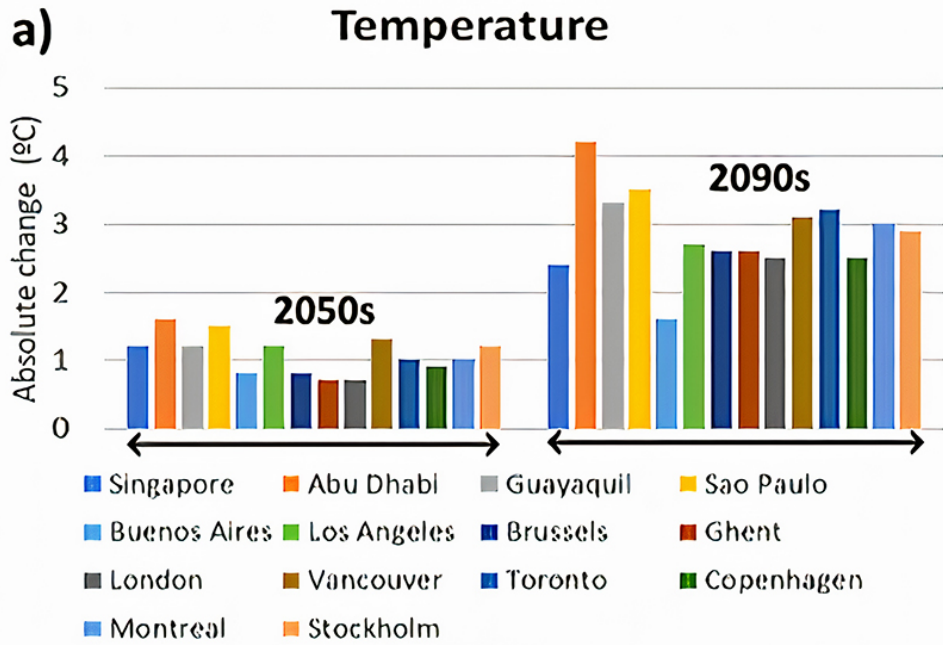


London

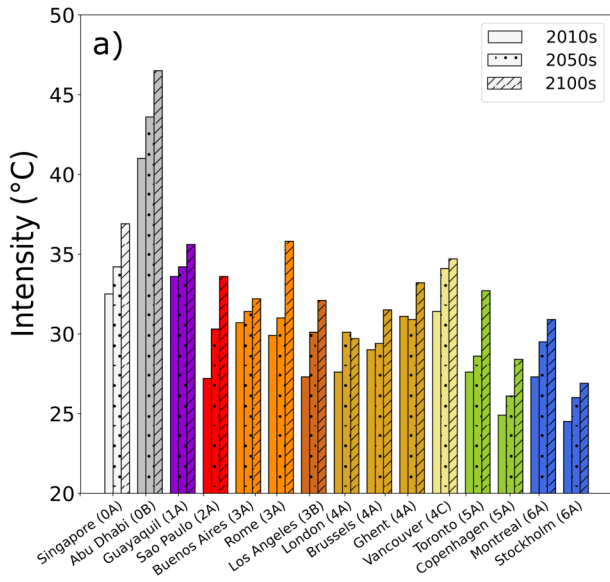


Toronto

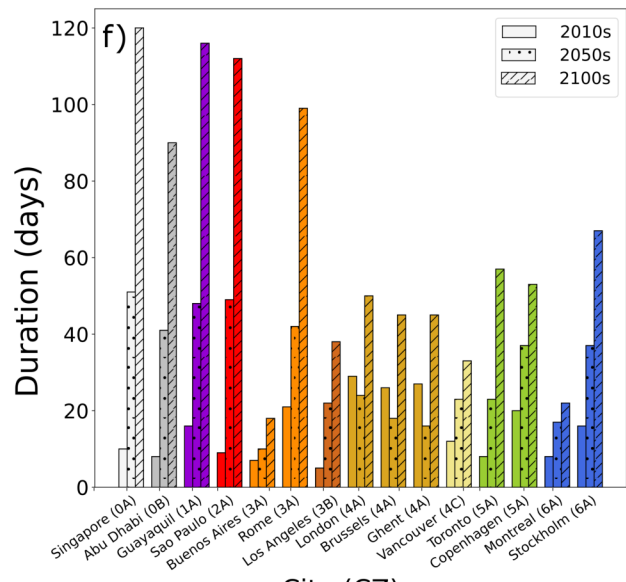
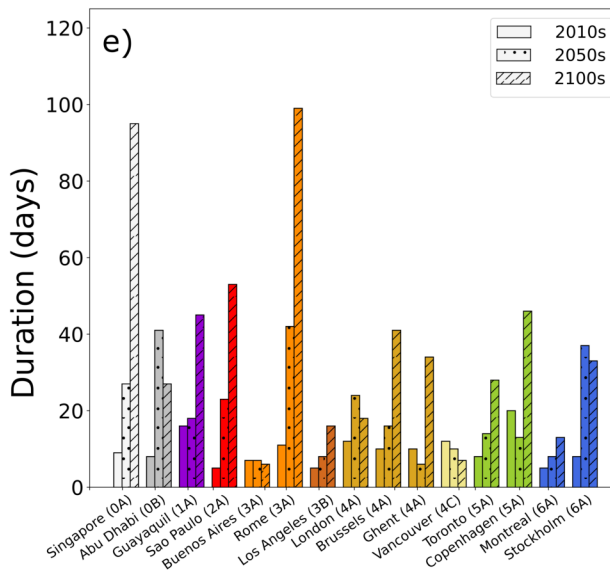
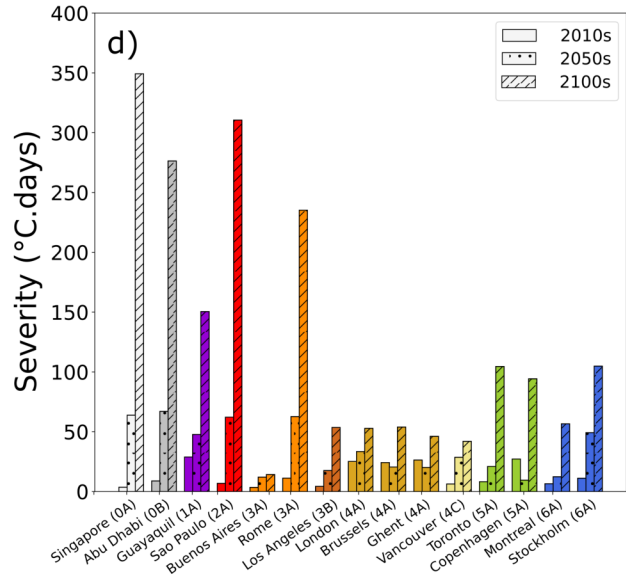
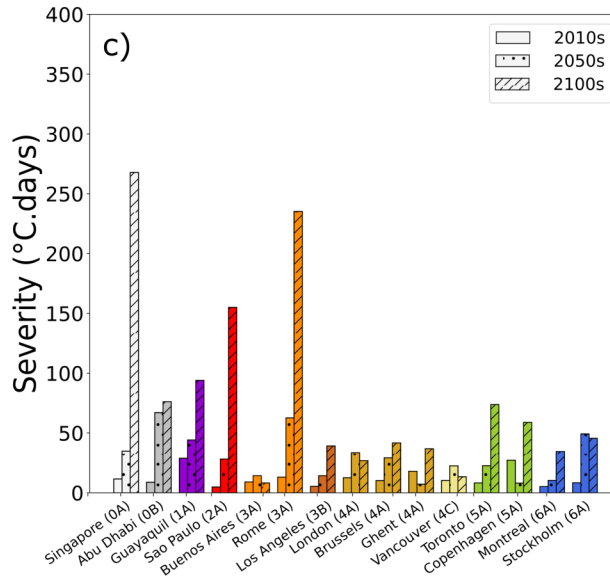
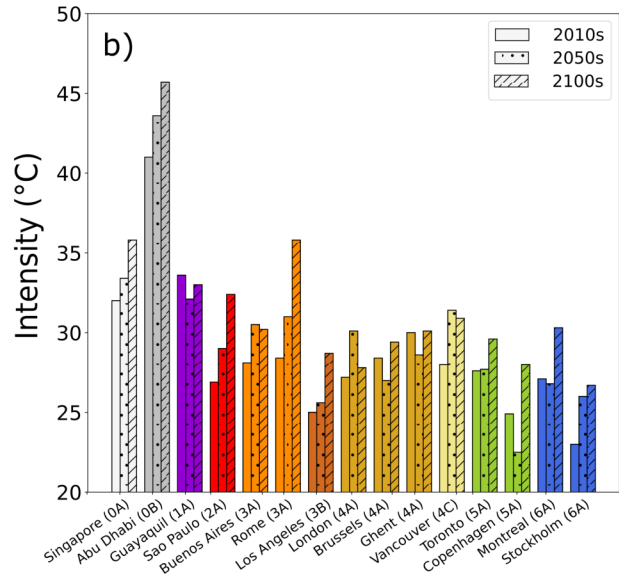




HWY : XTRM Most Intense



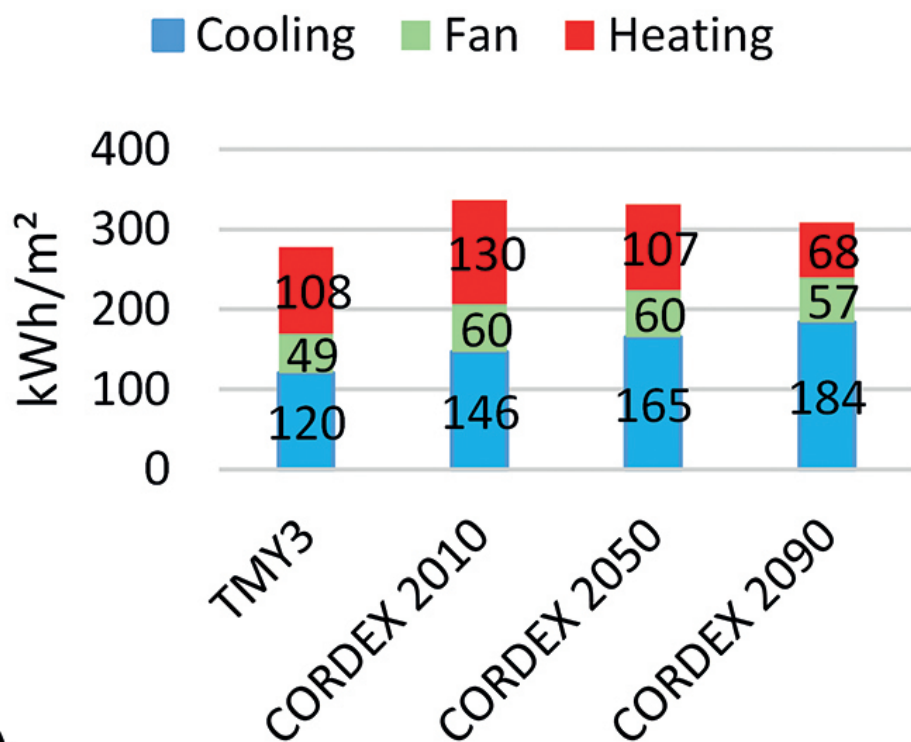
HWY : XTRM Longest



City (CZ)

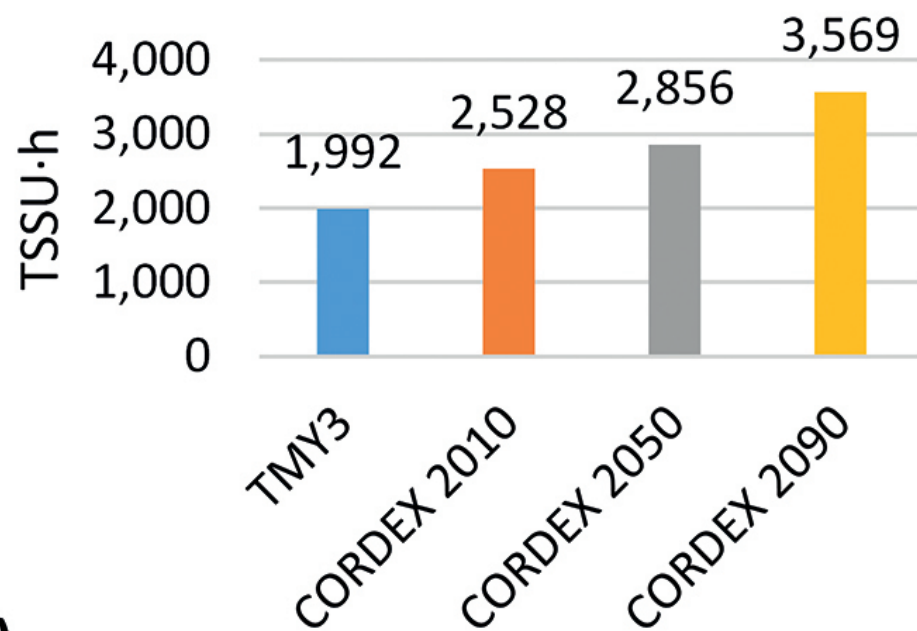
City (CZ)

Baseline annual HVAC primary energy use intensity



(A)

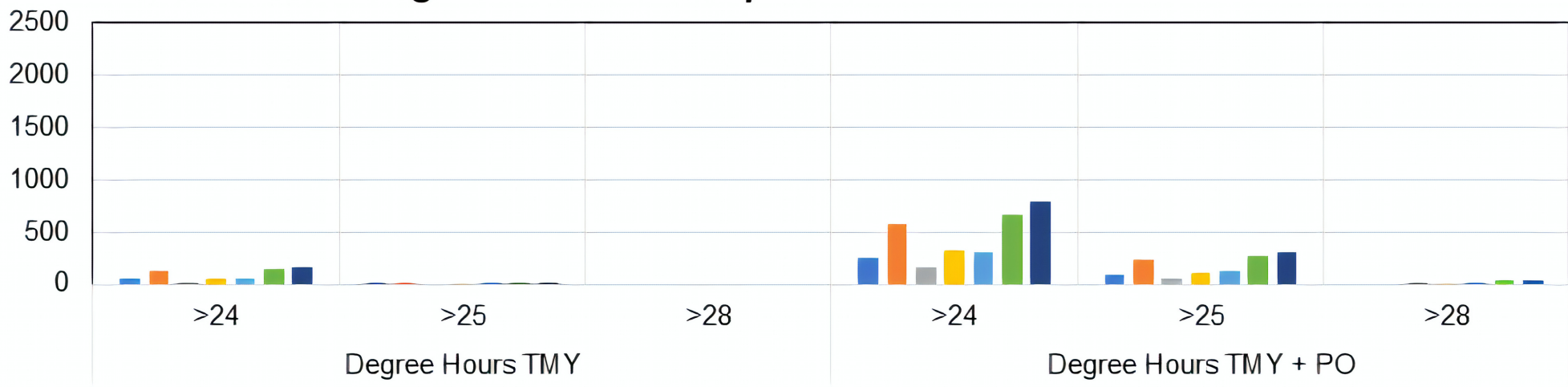
Baseline annual PMV-PPD model-based TSSU-weighted warm discomfort exceedance hours



(B)

E120 : Unmet Degree Hours for TMY period

1A 1B 2A 2B 2C 3A 3B



E120 : Unmet Degree Hours for Heatwave period

1A 1B 2A 2B 2C 3A 3B

